NASA CR-542-46
SDC-PJ-03

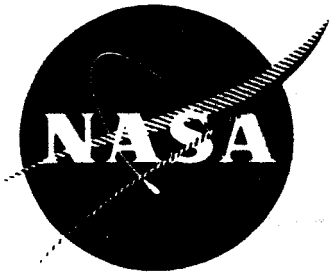

GPO PRICE $ _____

OTS PRICE(S) $ _____

Hard copy (HC) 4.00

Microfiche (MF) .75

DOUBLE DISCHARGE FEASIBILITY

by

M. L. Ghai and N. A. Pena

prepared for

NATIONAL AERONAUTICS AND SPACE ADMINISTRATION

CONTRACT NAS 8-2557

PLASMAJET SYSTEMS DIVISION
Space Dynamics Corp.
Cincinnati, Ohio

NASA CR-54246
SDC-PJ-03

SUMMARY REPORT

DOUBLE DISCHARGE FEASIBILITY

by

M. L. Ghai and N. A. Pena

prepared for

NATIONAL AERONAUTICS AND SPACE ADMINISTRATION

May 31, 1965

CONTRACT NAS 8-2557

Technical Management
NASA Lewis Research Center
Cleveland, Ohio

SPACE DYNAMICS CORP.
PLASMAJET SYSTEMS DIVISION
2215 Florence Avenue
Cincinnati 6, Ohio

TABLE OF CONTENTS

Section 4 EXPERIMENTAL STUDY

END

FORWARD

The contract was monitored by the Lewis Research Center, with Mr. Harold Ferguson as technical monitoring officer.

The major contributing technical personnel of the Plasmajet Systems Division, Space Dynamics Corporation were Mr. Norbert Pena, Mr. Robert Sparka and Dr. Mark Ghai.

Section 1 SUMMARY

Concept

The concept consists of accelerating a propellant with a suitable subsonic discharge and a supersonic discharge, with the objective of having flexibility of good performance in a wide range of specific impulse, particularly the range of 1500 to 5000 seconds, (Section 2)

Analysis

As a first step, a preliminary analysis has been carried out considering only the acceleration due to electro-thermal effects. Even under this restriction, appreciable gains in specific impulse and efficiency were indicated by theoretical calculations.

Analysis indicated increase of 25 to 100 percent in I_s corresponding to β values of 1 to 4, where β is the ratio of maximum propellant temperature in the supersonic discharge to the subsonic discharge (Fig. 6). Mollier chart analysis with specific impulse up to 4800 seconds has been presented (Table 3).

Two step energy addition also results in propellant temperature reduction, 30 to 40 percent for β of 1, giving an increase in efficiency from 32 to 55 percent under the frozen flows assumption, and from 74 to 75 percent under the shifting equilibrium flow assumption (Table 1).

Experiments

Preliminary experiments were conducted to determine the feasibility of operating a high pressure subsonic discharge in close proximity to another independent low pressure supersonic discharge. This feasibility was successfully demonstrated. It was confirmed not only by current readings and observation of spots of arc attachment, but also by measurement of heat transfer to segmented sections of the experimental unit.

The supersonic discharge was very stable, even more than the subsonic discharge. Arc attachment spots were visible for the subsonic discharge surfaces but not for the supersonic discharge, indicating that the supersonic discharge was well distributed over the electrode surface. Very high enthalpy levels were noted in some tests. The current and power levels in the two discharges could be varied. The unit could be operated with supersonic discharge alone, as well as with subsonic discharge alone, in addition to operation with both.

Considering the initial objectives and the available funds, the feasibility experiment was performed with nitrogen, using a water cooled copper unit.

Section 2 CONCEPT

Concept

In a Double Discharge Engine, energy is added to the propellant with the help of two controlled electric discharges, both within the same propellant accelerating channel. The first discharge is in the high pressure subsonic flow region, and the second is in the low pressure supersonic flow. Each discharge is independently controllable by varying the power input. Also each discharge can be operated singly.

Purpose

The purpose of this approach is:

(a) to attain specific impulse much above 2000 seconds, possibly 5000 seconds, with the help of a low pressure supersonic discharge eliminating the limitations imposed by the nozzle throat.

(b) to improve performance in the low specific impulse range of 1000 to 3000 seconds, by reducing the maximum propellant temperature and the associated dissociation losses,

(c) and, to provide an electric propulsion engine with inherent capability of good performance throughout the entire range of about 1000 to 5000 seconds.

Background

Consider first an engine using only a high pressure elctric discharge to heat the propellant which then is passed through the nozzle. This has been found to provide efficient operation at low specific impulse. The nozzle throat, however, becomes a limiting factor as the specific impulse is increased. The efficiency also decreases, due primarily to the high propellant temperatures and the associated dissociation losses.

These limitations can be removed if only part of the energy is added before the throat in the subsonic flow region, and the balance in the low pressure supersonic region. The engine is then no longer throat limited. Specific impulse is increased by increasing enthalpy after the propellant has passed through the throat. Figure 1 (a) shows schematically the variation of the propellant enthalpy in a single high pressure discharge engine at 1500 seconds, and Double Discharge engines operating at 1500 seconds and 5000 seconds.

The typical propellant temperature variation is shown in Fig. 1 (b). Because of the two step energy addition with intermediate cooling by expansion, the maximum propellant static temperature in a Double Discharge is less than for a single subsonic discharge. The dissociation losses are reduced, thereby improving the performance in the specific impulse range of 1000 to 3000 seconds.

Thus, it is hoped that high efficiency can be achieved in the specific impulse range of 1000 to 3000 seconds where dissociation energy plays an important part; yet, specific impulse on the order 5000 seconds can be achieved. In the lower part of the specific impulse range, energy needs to be introduced at high pressures to keep dissociation low, whereas in the higher portion of the range more energy is required in the supersonic discharge. Hence, the need for independently controllable discharges.

Consider next the other extreme, namely an engine using only low pressure supersonic discharge. High dissociation and ionization of the propellant is unavoidable. Such an engine is therefore limited to operation at high specific impulses only, where the dissociation and ionization energy can be considered negligible as compared to the total energy. The efficiency may be expected to drop rapidly at specific impulse levels below 5000 seconds.

Consider next the case where the arc travels from the anode in the high pressure subsonic flow, passes through the throat and terminates at the nozzle in the supersonic flow region. This has the advantage of imparting part of the energy after the nozzle throat; but, there are two limitations.

First, since voltage gradient in a discharge depends strongly on the pressure, most of the voltage drop and energy transfer takes place in the subsonic part of the discharge because of the high pressure, and only a small fraction of the power can be introduced into the supersonic region because of the low pressure. Only a small increase in specific impulse can therefore be expected, due to the supersonic portion of the discharge. Also, the location and quantity of energy input to various parts of the accelerating channel can not be controlled and varied.

Second limitation arises from the fact that in a single discharge, by necessity the same current must flow in the low pressure region as in the high pressure region. As a result, it is not possible to take advantage of one of the most attractive features of the low pressure supersonic discharge. When the pressure is low, there is a sheath-like discharge spread out evenly on the electrode surface as compared to the rod-like or column-like discharge at high pressures. This reduces current density, and decreases the heat flux. High currents in supersonic region may give some additional electromagnetic acceleration due to interaction with self induced magnet field; but, in any case, high currents in supersonic discharge are necessary if appreciable amount of power is to be introduced to attain high specific impulse.

These limitations can be removed if the two discharges are independent. High pressure discharge can then have low current levels and high voltage gradients, whereas the supersonic discharge higher currents at lower voltage gradients.

Improvement in electrode life may be expected when the current level in the high pressure discharge is reduced, as shown schematically in Fig. 1(c).

Fig. 2 shows schematically a typical electrode configuration and accelerating channel for Double Discharge Engine. Fig. 3 shows a cross section of the experimental unit used.

Main Program Objective

Although the Double Discharge Concept appeared to be attractive, it was unknown whether it would be feasible to operate and control two discharges in very close proximity, particularly if one discharge is required to be high pressure subsonic and the other is low pressure supersonic. There had been no known data on simultaneous operation of the subsonic and supersonic discharges on very close proximity.

The main objective of the work reported here was to determine if this was feasible.

NOMENCLATURE

θ - Temperature Difference

β - Reheat temperature ratio - that is, ratio of the maximum static temperature during the second energy addition to the maximum static temperature during the first energy addition.

γ - Ratio of specific heats

η - Energy Efficiency

α - Degree of dissociation of propellant

A - Area of cross section

c - accoustic velocity

c_p - Specific heat at constant pressure

g - Gravitational constant

H, h - Enthalpy

I - Specific Impulse

J - Mechanical Equivalent of Heat
q - Heat Flow Rate
Q - Heat Flow

$\bar{R}$ - Gas Constant

R - Ratio of Specific Impulse of Double Arc to specific Impulse of single arc

T - Temperature

U - Internal Energy

V - Gas velocity

$\dot{\omega}$ - Propellant Flow Rate

Subscripts

sub - Subsonic Arc
sup - Supersonic Arc

i - intermediate pressure

d - Double Arc
s - Single Arc
o - Outside

Section 3 ANALYTICAL STUDY

The analytical study consists of four parts. In the first three parts, mathematical analysis has been made with simplifying assumptions. In the fourth part, numerical analysis using hydrogen as propellant and working with Mollier charts to take a real case, has been presented.

Section 3.1 THEORETICAL SPECIFIC IMPULSE

Assumptions

The propellant is assumed to be an ideal gas - that is there is no dissociation, ionization, or other real gas effects.

The specific heat is taken constant. The expansion in the nozzle is taken as an adiabatic isentropic process. The energy addition by the arc is taken as a constant pressure heating process.

Under these assumptions, the performance of a Double Arc and a single arc unit has been compared.

Generalized Expression

The Double Arc engine may be considered to have three distinct thermodynamic regions, as shown in Fig. 4.

In the first region, energy is added to the propellant by the subsonic arc, and the propellant expanded in the nozzle up to sonic velocity.

In the second region, further expansion takes place and there is simultaneous addition of energy by the supersonic arc. The rates of expansion and energy addition must be such that the flow does not become subsonic or sonic.

In the third region, propellant expands further to the discharge pressure.

On the H-S diagram, Fig. 4, the operation in the first region may be shown by lines 0-1 and 1-3. The gas velocity, neglecting the initial velocity, is given by

$$\frac{V_3^2}{2\,g\,J} = h_1 - h_2 = c_p\,(T_1 - T_2) \qquad (1)$$

The operation of the second region follows a line such as the line $3 - 4$, representing reheating of the fluid and simultaneous expansion to a lower pressure to keep the flow supersonic. The energy balance for the second region gives

$$\frac{V_4^2}{2\,g\,J} - \frac{V_3^2}{2\,g\,J} = Q_{sup} - c_v\,(T_4 - T_3) - (P_4 v_4 - P_3 v_3) \qquad (2)$$

The operation of the third region is represented by line $4 - 2$. The velocity increase in this region is given by

$$\frac{V_5^2}{2\,g\,J} - \frac{V_4^2}{2\,g\,J} = h_5 - h_4 = c_p\,(T_5 - T_4) \qquad (3)$$

The engine exit velocity is obtained by adding Equations (1), (2), and (3).

$$\frac{V_5^2}{2\,g\,J} = c_p\,(T_1 - T_3) + c_p\,(T_2 - T_4) + Q_{sup} - c_v\,(T_4 - T_3) - (p_4\,v_4 - p_3\,v_3) \qquad (4)$$

$$I_s = \frac{c}{g}$$

Taking $p_e = 0$ for space propulsion, specific impulse is given by

$$I_s = \frac{p_2\,A_2}{w} + \frac{(2\,g\,J)^{1/2}}{g}\left[c_p\,(T_1 - T_3) + c_p\,(T_2 - T_4) + Q_{sup} - c_v\,(T_4 - T_3) - (p_4\,v_4 - p_3\,v_3)\right]^{1/2} \qquad (5)$$

Constant Pressure Supersonic Arc

This generalized expression becomes quite simple if it is assumed that energy addition by the supersonic arc takes place at constant pressure.

Equation (5) then becomes,

$$I_s = \frac{p_2 A_2}{\dot{\omega}} + \frac{2 g J}{g} \left[c_p (T_1 - T_3) + c_p (T_4 - T_5) + (c_p - c_v)(T_4 - T_3) - (p_4 v_4 - p_3 v_3) \right]^{1/2}$$

Substituting $pv = RT$ and $R = c_p - c_v$, it gives

$$I_s = \frac{p_2 A_2}{\dot{\omega}} + \frac{(2 g J)^{1/2}}{g} \left[c_p (T_1 - T_3) + c_p (T_4 - T_3) \right]^{1/2} \qquad (6)$$

Comparison with Single Arc Engine - Specific Impulse Ratio

Comparing this with the single arc engine, operating between the same overall pressure ratio and having the same total enthalpy at the throat, we have for the single arc engine

$$I_s = \frac{p_2 A_2}{\dot{w}} + \frac{(2 g J)^{1/2}}{g} \left[c_p (T_1 - T_2) \right] \qquad (7)$$

The increase in specific impulse obtained by the use of double arc may be expressed by the ratio R, that is the ratio of specific impulse of double arc engine to that of single arc engine, and may be obtained from Equations (6) and (7).

If $\frac{p_2 A_2}{\dot{w}}$ is negigible as compared to the second term

in Equations (6) and (7), the ratio R, comparing the Specific Impulse of Double Arc to Single Arc, is given by,

$$R^2 = \frac{c_p (T_1 - T_3) + c_p (T_4 - T_3)}{c_p (T_1 - T_2)} \qquad (8)$$

$$= \frac{(h_1 - h_3) + (h_4 - h_5)}{(h_1 - h_2)}$$

Also,

$$R^2 = \frac{c_p T_1 \left[1 - \left(\frac{pi}{p_1} \right)^{\frac{v-1}{v}} \right] + c_p T_4 \left[1 - \left(\frac{p_2}{pi} \right)^{\frac{v-1}{v}} \right]}{c_p T_1 \left[1 - \left(\frac{p_2}{p_1} \right)^{\frac{v-1}{v}} \right]} \qquad (9)$$

p_1 is the intermediate pressure at which the supersonic arc discharge is assumed to take place.

Optimization of Supersonic Arc Pressure

To determine optimum pressure, Equation 9 may be differentiated with respect to p_i. The condition for optimum operation is obtained as

$$\frac{\left(p_i\right)^{\frac{\gamma-1}{\gamma}-1}}{\left(p_1\right)^{\frac{\gamma-1}{\gamma}}} = \beta \frac{\left(p_2\right)^{\frac{\gamma-1}{\gamma}}}{\left(p_i\right)^{\frac{\gamma-1}{\gamma}+1}}$$

where $\beta = \frac{T_4}{T_1}$. This gives,

$$(p_i)^2 = (\beta)^{\frac{\gamma}{\gamma-1}} (p_1 - p_2) \qquad (10)$$

$$\left(\frac{p_i}{p_1}\right) = (\beta)^{1/2} \cdot \frac{\gamma}{\gamma-1} \left(\frac{p_2}{p_1}\right)^{-/2}$$

$$\left(\frac{p_2}{p_1}\right) = (\beta)^{1/2} \frac{\gamma}{\gamma-1} \left(\frac{p_2}{p_1}\right)^{1/2}$$

Substituting these in Equation (9),

$$R^2 = 1 + \frac{\left(\sqrt{\beta} - x\right)^2}{1 - x^2} \qquad (11)$$

where $x = \left(\frac{p_2}{p}\right)^{1/2} \frac{\gamma-1}{\gamma}$

Effect of Reheat Factor and Pressure Ratio

The above equation shows that R will always be greater than one since the term $(\beta^{1/2} - x)^2$ will always be positive. Thus, the specific impulse of Double Arc will always be greater than the specific impulse of the Single Arc engine.

The equation also indicates that the advantage to be gained by the use of the Double Arc depends upon β as well as p_2 / p_1.

The effect of β may be first seen by assuming the nozzle exit pressure is near zero, and substituting $p_2 / p_1 = 0$ in Equation (11), gives

$$R = (1 + \beta)^{1/2} \qquad (12)$$

where $$\beta = \frac{T_4}{T_1}$$

The increase in specific impulse can be expressed by a very simple expression.

Increase of specific impulse for the ideal case of a nozzle with infinite expansion ratio, is shown in Fig. 5 as a function of β.

In a nozzle, the heat flux to the nozzle wall falls rapidly after the throat. This is due to the rapidly decreasing pressure, increasing diameter, and decreasing recovery temperature. The upper limit on reheat temperature is reached when the heat flux from the reheated gas equals the cooling capability. Values of β much greater than 1 should be possible although the upper practical limit is not known.

Nozzle with Limited Pressure Ratio

For a nozzle with pressure ratio of 1000, the specific impulse increase has been shown in Fig. 6 for a diatomic propellant (hydrogen) as well as a monatomic propellant, (lithium).

3.2 PROPELLANT TEMPERATURE

A predominant source of energy loss in a high specific impulse arc engine is the loss due to dissociation and ionization of the propellant. The effect of use of Double Arc on this loss is considered next.

The maximum propellant temperature in a Double Arc engine is less than the temperature in the single arc engine operating at the same specific impulse.

Double Arc Propellant Temperature

Using subscripts s for single and d for double arc; for the two engines operating at the specific impulse, the temperatures at locations shown on Fig. 4 are as follows

$$(T_{1,d} - T_2) = (T_{1,s} - T_3) + (T_4 - T_5)$$

$$\frac{T_{1,d}}{T_{1,s}} = \frac{1 - \left(\frac{p_2}{p_1}\right)^{\frac{\gamma-1}{\gamma}}}{\left[1 - \left(\frac{p_i}{p_1}\right)^{\frac{\gamma-1}{\gamma}}\right] + \beta\left[1 - \left(\frac{p_2}{p_i}\right)^{\frac{\gamma-1}{\gamma}}\right]} \qquad (13)$$

Double Arc With Equal Expansion Ratios

Assuming equal pressure ratios for the two arcs and substituting for π, Equation (13) becomes

$$\frac{T_{1,d}}{T_{1,s}} = \frac{1 - x^2}{(1 - x) + \beta (1 - x)}$$

where $$x = \left(\frac{p_2}{p_1}\right)^{1/2 \cdot \frac{\gamma - 1}{\gamma}}$$

$$\frac{T_1, d}{T_1, s} = \frac{1 + x}{1 + \beta} \qquad (14)$$

Since, for values of $\beta > 1$, the maximum temperature in the supersonic stream of the Double Arc engine is greater than the maximum temperature in the subsonic region, it is also important to compare the maximum supersonic temperature with the corresponding maximum propellant temperature in the single arc engine.

$$\frac{T_4, d}{T_1, s} = \frac{\beta (1 + x)}{(1 + \beta)} \qquad (15)$$

Temperature Reduction

The maximum propellant temperatures have been plotted in Figure 7, for a monatomic propellant.

It is interesting to note that the propellant temperatures are reduced, not only in the subsonic regime (T_1, d) but also in the supersonic region, (T_4, d). Even when the supersonic reheat is up to twice the initial temperature, that is $\beta = 2$, the maximum temperatures are kept less than the temperatures required in the single arc engine.

Figure 8 shows a similar plot of propellant temperatures for a diatomic propellant. At the same specific impulse level, the propellant temperatures are reduced in the Double Arc.

3.3 EXPANSION EFFICIENCY

Theoretical Efficiency

Next, consider conversion of thermal energy to kinetic energy. Ideal conditions of isentropic adiabatic expansion, and ideal gas propellant are assumed, as before.

The ideal cycle efficiency for a system with maximum temperature T_1 and heat rejection temperature T_2 is given by

$$\eta = \frac{T_1 - T_2}{T_1}$$

Thus efficiency of a single arc engine may be written in terms of symbols of Fig. 4 as

$$\eta_s = 1 - \frac{T_2}{T_{1,s}} \tag{16}$$

A similar expression for the Double Arc is,

$$\eta_d = \frac{\left(1 - \frac{T_3}{T_{1,d}}\right) + \beta\left(1 - \frac{T_5}{T_4}\right)}{\left(1 - \frac{T_3}{T_{1,d}}\right) + \beta} \tag{17}$$

If the expansion ratios of the two stages of the Double Arc engine are assumed to be equal, this gives

$$\eta_d = 1 - \frac{\beta \left(\frac{T_3}{T_1}\right)}{1 + \beta - \left(\frac{T_3}{T_1}\right)} \qquad (18)$$

Comparison with Same Pressure Limits

The pressure ratio for the Single Arc engine is p_2 / p_1 . The pressure ratio for each stage of the Double Arc, assuming again equal pressure ratios in the two stages, is given by

$$\frac{p_2}{p_i} = \frac{p_i}{p_1} = \left(\frac{p_2}{p_1}\right)^{1/2}$$

Substituting in the expression for Double Arc efficiency, and rearranging gives

$$\eta_d = \frac{1 - x}{1 + \frac{1}{1+\beta}\, x} \qquad (19)$$

For the Single Arc engine,

$$\eta_s = 1 - x^2 \qquad (20)$$

Figure 9 gives a comparison of efficiencies at different overall pressure ratios, for $\beta = 1$.

It is noted that the efficiency of the Double Arc on this basis is somewhat less than the efficiency of the Single Arc. This remains true even if allowance is made of the fact that the thrust due to exit pressure p_2, is somewhat larger for the double arc than for the single arc. This allowance for exit thrust was computed from the following

$$\eta_s = 1 - \frac{x^2}{\gamma} \tag{21}$$

$$d = \frac{(1 - x) + \left(\frac{\gamma - 1}{\gamma} \cdot \frac{p_2}{1 + \beta}\right) x}{1 - \frac{x}{1 + \beta}} \tag{22}$$

Equations (21) and (22) have been plotted in Fig. 9.

Comparison With Same Temperature Limits

From the point of view of efficiency it is desirable that the overall pressure ratio be higher for the Double Arc than for the Single Arc, so that each stage can operate at appropriate pressure ratio. For instance, Expansion ratio of 2500 for the Double Arc will give an expansion ratio of 50 for each stage, assuming equal pressure ratio across each stage.

In the absence of knowledge of optimum pressure ratios for the Double Arc, it was considered desirable to make a comparison on the basis of the same maximum enthalpy in the chamber. Also the same enthalpy level is assumed at the exit. This is based on the assumption that the cut-off point for expansion is decided on the basis of reaching a certain enthalpy level rather than a certain pressure.

For constant specific heat, this amounts to comparison on the basis of the same maximum and minimum gas temperatures.

$$T_1 = T_{1,s} = T_4 = T_{1,d}$$

$$T_2 = T_5$$

Substituting these in Equations (16) and (17),

$$\eta_s = 1 - \frac{T_2}{T_1}$$

$$\eta_d = 1 - \frac{\frac{T_2}{T_1}}{2 - \frac{T_2}{T_1}} \qquad (23)$$

Equation 23 has been plotted in Figure 10 for differenct values of T_1 / T_2. Under these conditions, the efficiency of the Double Arc is found to be somewhat higher than for the single arc.

Both Figures 9 and 10 are under the assumption of ideal fluid neglecting dissociation and ionization of the propellant. Therefore, they are of somewhat academic interest only. To obtain a more realistic picture of efficiency, comparison was then made with the use of Mollier diagram taking into account the propellant dissociation and ionization.

3.4 NUMERICAL ANALYSIS WITH MOLLIER CHART

Numerical analysis of typical operating points of single and Double Discharge engines was conducted, using Mollier Chart for hydrogen.

Comparison at Same Specific Impulse

Table 1 gives a comparison for engines operating at approximately the same specific impulse, on the order of 1200 seconds.

It is seen that, for approximately same specific impulse, the maximum propellant temperature required for the Double Discharge is 3000°K as against 4000°K for the single discharge. The efficiency increases from 32 to 55 percent for the frozen flow, due primarily to the reduced dissociation levels corresponding to lower propellant temperature.

Single arc engine with T_1 of 4000°K gives specific impulse of 900 seconds and 1370 seconds, for frozen flow and shifting equilibrium flow, respectively.

For the Double Arc engine to operate at about the same specific impulse, Fig. 8 indicates a temperature ratio of 6.5 for β=1. The temperature required for ideal cycle double arc (without allowance for energy losses due to dissociation), is 0.65 x 4000 = 2600°K. In the example shown, T_1 of 3000°K, and reheat temperature of 3000°K, was assumed.

According to Fig. 8, the theoretical efficiency of a single arc engine for pressure ratio of 1000 is 86 percent. For a Double Arc engine, with the same pressure ratio, the theoretical expansion efficiency is 77 percent. The Mollier Diagram analysis changes the expected performance values primarily due to dissociation effects. The maximum propellant dissociation for the single arc engine at 4000°K is 24 percent, whereas the maximum dissociation at 3000°K required for the Double Arc engine is only 8.5 percent. As a result the actual efficiency does not decrease in accordance with Fig. 8. Actually the efficiency increases from 35 to 50% for the frozen flow case, and remains approximately same (74 versus 75) for the shifting flow case.

Two extreme cases of frozen and shifting equilibrium flow bracket the actual performance.

Table 1 Comparison of Performance of Double Discharge Virsus Single Discharge at Approximately Equal Specific Impulse - Note The Reduction In Propellant Temperature and Increase In Efficiency.

	Single Discharge		Double Discharge	
	Frozen Equilibrium	Shifting Equilibrium	Frozen Equilibrium	Shifting Equilibrium
Temperature, T_1, °K °K	4000	4000	3000	3000
Pressure, P_1, ^{1}atm	10	10	10	10
H_1/RT_o	108	108	45	45
Dissociation, 1, %	24	24	4	4
Frozen H $1/RT_o$	46	46	8	8
Pressure, P_2, atm	.01	.01		
H_2/RT_o	28	28		
Intermediate Press, Pi, atm			1	1
H_3/RT_o			25	25
H_4/RT_o			60	60
Dissociation, 4, %			8.5	8.5
Frozen H $4/RT_4$			16	16
Pressure, P_5, atm			.01	.01
H_5/RT_o			20	20
Total H/RT_o added	108	108	80	80
Available H/RT_o	34	80	44	60
Specific Impulse, Sec	900	1370	1030	1220
Efficiency, %	32	74	55.0	75

Comparison with Same Maximum Dissociation Level and Same Temperature Limits

Next, Mollier Chart analysis is made of engines having same temperatures of heat addition and heat rejection. According to Fig. 10 the efficiency of the Double Arc engine is somewhat higher than the single arc engine, operating at same T_1 and T_2. In the examples shown in Table 2, T_1 is 4000°K and T_2 is 2000°K for both the engines.

The reheat temperature of 3400°K is selected so that the maximum dissociation after reheat is same as the dissociation at the end of the first heating cycle, 24 percent in each case.

It is noted from Table 2 that the shifting flow efficiency increases from 74 to 78 percent. The frozen flow efficiency increases from 31 to 42 percent.

According to Fig. 6 for operation with hydrogen at B of 3400/4000 or 0.85, the specific impulse increase to be expected is 16 percent.

The specific impulse increases from 1370 to 1550 for the shifting equilibrium case and from 895 to 1130 seconds for the frozen flow case. The specific impulse increases 13 percent for the shifting case, and 26 percent for the frozen flow case.

Table 2 Comparison of Performance of Double Discharge Virsus Single Discharge at Equal Maximum Dissociation Level and Same Temperature Limits. Note The Increase In Specific Impulse and Efficiency.

	Single Arc		Double Arc	
	Frozen Equilibrium	Shifting Equilibrium	Frozen Equilibrium	Shifting Equilibrium
Max. Temp., T_1, °K	4000	4000	4000	4000
Min. Temp., T_2, T_4, °K	2000	2000	2000	2000
Max. Dissociation, , %	24	24	24	24
P_1, atm	10	10	10	10
H_1/RT_o	108	108	108	108
Dissociation 1, %	24	24	24	24
Frozen H 1/RT_o	46	46	46	46
P_2, atm	.01	.01		
H_2/RT_o	28	28		
Dissociation 2, %	3	3		
Frozen H 2/RT_o	6	6		
Pi, atm			1	
H_3/RT_o			71	
Reheat T_4, °K			3400	
H_4/RT_o			95	
Dissociation, 4, %			24	
Frozen, H 4/RT_o			46	
T_5, °K			2000	
H_5/RT_o			.003	

	Single Arc		Double Arc	
	Frozen Equilib-rium	Shifting Equilib-rium	Frozen Equilib-rium	Shifting Equilib-rium
Total H/RT_o Added	108	108	132	132
Unav. Exhaust H/RT_o	28	28	30	30
Add'l Frozen H/RT_o	46	--	46	--
Available H/RT_o	34	80	56	102
Specific Impulse, Secs	895	1370	1130	1550
Efficiency, %	31	74	42	78

HIGH SPECIFIC IMPULSE ENGINE

The effect of variation of intermediate pressure for the double arc engine, and the quantity of energy addition in the second stage, are shown in Table 3.

Without exceeding the heat flux limitations, the reheat temperature can be much higher than the first stage temperature because of lower pressure.

Table 3 indicates specific impulse up to 4800 seconds with electrothermal effects only.

Table 3 High Specific Impulse Double Discharge Engine - Variation of Quantity and Location of Energy Addition in the Supersonic Discharge

	DOUBLE DISCHARGE		
	Operation I	Operation II	Operation III
First Discharge			
T_1 °K	5500	5500	5500
P_1, atm	31.5	31.5	31.5
H_1/RT_o	228	228	228
First Expansion			
P_4, atm	3.15	3.15	$(10)^{-1}$
H_3/RT_o	165	165	105
Second Discharge			
H_4/RT_o	210	360	1570
T_4, °K	4500	9000	14,500
Second Expansion			
P_5, atm	$(10)^{-4}$	$(10)^{-4}$	$(10)^{-4}$
H_5/RT_o	50	110	740

	DOUBLE DISCHARGE			
	Operation I	Operation II	Operation III	
Total Performance				
H/RT_o Added	273	423	1693	
H/RT_o Avail	223	313	953	
Efficiency	81	74	56	
Specific Impulse	2300	2750	4800	

Section 4 EXPERIMENTAL STUDY

4.1 TEST UNIT

Experimental Units

Two units were designed to conduct tests. The first engine was designed to operate at high wall temperatures, using Lithium or Hydrogen as coolant. All the components of the engine were of refractory materials compatible with Lithium.

This design is shown in Figs. 12 to 14. Figure 12 shows the high pressure end of the engine, making provision for electrode leaks, electrode gap adjustment, high pressure containment without leaks, and lithium vapor control. The engine head was designed to enable separate calorimetric measurements for heat flux to the subsonic and supersonic electrodes and nozzle.

The subsonic and supersonic electrodes are shown in Figs. 13 and 14. The tubular design of electrodes enabled measurement of the temperature rise of the coolant, and the coolant flow rate, so that heat flux to each electrode could be determined separately. The major problem was to get thin walled tubes of refractory materials, and to fabricate an assembly of rather small dimensions. These were overcome by appropiate design approaches, using electron beam welding.

The second engine was designed to operate at comparatively low wall temperatures, using copper throughout and employing water cooling. An assembly of the unit is shown in Fig. 3.

Nozzle Segmentation

A unique feature of this design was the segmentation of the nozzle into four sections, separated by thin insulating washers. The segmented sections were (1) propellant feed, (2) subsonic arc and nozzle throat, (3) supersonic arc portion of the divervent section of the nozzle, (4) and, the final expansion portion of the divergent section of the nozzle. The segmentation of the nozzle was considered an important, almost necessary, step to accomplish the test objectives.

It was felt that for the Double Arc to be most effective, it is not only necessary to be able to operate two independently controlled arcs, but also to make sure that the supersonic arc operates within a limited portion of the divergent portion of the nozzle, so that there is after-expansion at the end of supersonic heating. It would not be desirable to have supersonic arc attached at the exit end of the nozzle. Segmentation of the divergent part of the nozzle was used to determine whether the supersonic arc strikes where it should.

The second objective of nozzle segmentation was to be able to assess the heat flux to the part of the nozzle where the supersonic arc strikes, to determine the distribution of heat flux in a nozzle with subsonic and supersonic arcs, and to compare it with a nozzle having subsonic arc only.

The operation of segmented nozzle was made possible by the use of water cooled copper walls so that the insulators dividing the segments could be kept at low temperature, through contact with cooled copper.

The design of the pin electrodes for the copper engine was similar to that shown in Figs. 13 and 14, using tubular construction. For each electrode, the water flow and the temperature rise could be measured separately.

Research Unit

Considering the desired initial program objectives and the available funds, the work reported here was conducted with water cooled copper engine.

The research unit is shown in the upper half of Fig. 15. The segmented nozzle design can be easily seen. The two pin electrodes and the various nozzle segments have independent coolant supply.

The research engine is shown mounted to the vacuum tank in the lower half of Fig. 15.

Research Fluid

Although a lithium or hydrogen engine was not used, it was considered desirable that the Double Arc ignition feasibility testing should be done with a fluid as close to hydrogen as possible. Nitrogen has ionization potential nearly the same as hydrogen. It is diatomic like hydrogen so that the effect of dissociation of an arc stability would be simulated, at least partially. Nitrogen was therefore selected as the working fluid. Preliminary stability checks were made with Argon.

4.2 TEST SET-UP AND INSTRUMENTATION

A schematic of the electrical test set up is shown in Fig. 16. Each arc had a separate ballast and a separate electrical circuit. The voltage at the electrodes could be varied on the positive side as well as on the negative side. The object was to obtain a good degree of flexibility of operation.

Ballasts used in the experiment are shown in Fig. 17. This figure also shows the flow control consoles used.

A typical test set up is shown in Fig. 18, except for the thrust measuring device which was not required in the current experiments. The photograph also shows the end of the vacuum tank where the unit was mounted. The vacuum tank was approximately 4 feet in diameter by 13 feet length.

Instrumentation

The coolant and propellant flow were measured by Fischer Porter gages, with accuracy of 0.2% of scale. This amounted to an accuracy of 0.4 to 1 percent for the range of measurement. Prior to delivery of the coolant flow meters, some tests were run with the technique, of collecting and weighing the coolant from all the five circuits individually.

When several electrical potentials are involved, the measurement of temperatures by conventional thermocouples often gives difficulties, and erroneous results due to stray currents. These were overcome by using direct reading thermometer gages employing thermal sensing elements rather than electrical sensing elements. The thermometer gages had an accuracy of 2 percent and divisions of 1°F.

To determine the flow characteristics of the propellant gas feed system, the pressure drop was measured for different flow rates. This was used to determine the true arc chamber pressure, from pressure gage measurements taken at the flow meter on the instrument console.

The voltmeters and the ammeters used had an accuracy of $\pm$ 2%.

The enthalpy was measured by the heat balance method. The energy input was measured by the D.C. voltmeters and ammeters. The losses were measured by the coolant flow rate and its temperature rise.

4.3 TEST SET UP CHARACTERISTICS

Prior to taking heat flux data, tests were run to insure that the thermal characteristics of the test apparatus were suitable for taking accurate data.

Thermal Equilibrium Characteristics

Transient characteristics of the system during a typical visit are shown in Fig. 19.

Figure 19 shows that about 10 seconds were required for ignition and operation of both the arcs. The coolant temperatures for the subsonic and supersonic electrodes would reach near equilibrium condition in about 30 seconds. The nozzle segments, however, took a little longer to reach equilibrium, generally on the order of 60 seconds.

Most of the tests were run for 1-1/2 minutes to 4 minutes, although in some cases, the unit was run as long as 7 minutes at a time.

The coolant flow had two circuits with a flow meter in each circuit, in most of the tests. The flow in the first circuit passed through the supersonic pin electrode, while the flow in the other circuit passed through the rest of the cooling segment. Because of the narrow coolant passages in the supersonic pin electrode, and the resultant pressure drop, it was necessary to have an independent circuit for the supersonic pin electrode to have adequate flow rate.

The unit was usually stopped immediately after the necessary data had been taken. Running of the unit for long periods generally resulted in a breakdown of the boron-nitride insulation sleeve between the pin electrodes, as well as the insulators between the nozzle segments. It will be recalled that the nozzle had been segmented to accurately determine the location of arc attachment and also for heat flux distribution data.

Thermal Loss Characteristics

In order to minimize the thermal loss from the tubes carrying the coolant from the engine to the temperature sensing elements, and the flow meters, the tubes were of insulating materials (rubber) and the valves were lagged with insulation. It was, however, not convenient to insulate the exposed parts of the engine or the engine leads.

The thermal loss from the various parts of the system was computed by the well known heat transfer relationship (see Appendix 1), and the results are presented in Fig. 20.

4.4 TEST RESULTS

Preliminary

After checking out the engine for possible leaks, coolant flow obstructions, electrical insulation, etc., the subsonic arc was run alone, operating as a conventional arc jet. The tests indicated that the engine design was generally satisfactory. The arc ignited and operated well. Starting was done by lowering the pressure below the breakdown value Sometimes a high frequency ignitor was used.

Tests were then run with the supersonic arc alone. Except for some difficulties due to mishaps resulting from inadvertent operation with coolant valves closed, the supersonic arc discharge worked well in a stable manner.

Double Arc Operation Feasibility

Several tests were then conducted with both the subsonic and supersonic arcs to determine the feasibility of ignition and simultaneous operation of both the arcs. The observations made during attempts to run both arcs are summarized below.

The supersonic arc was found to be surprisingly very stable - even more than the subsonic arc. Normally, this would be advantageous and desirable; however, in the present design it sometimes created difficulties of maintaining the subsonic arc. The entire discharge tended to accumulate in the supersonic arc. This was prevented by suitable adjustment of the arc gap.

The high degree of stability of a supersonic arc has not been reported in literature previously, to the best of our knowledge. This was an unexpected discovery since it was originally felt that very high gas velocities in the supersonic region might tend to overcool the arc column and make the arc discharge unstable.

Experimental engine and the test set up had been so designed that the potential of each of the four electrode terminals, two pin electrodes and two nozzle electrodes, could be independently controlled. The "floating" surfaces could be made to assume any desired voltage. The voltage of various surfaces was varied with respect to each other. Interestingly, three arcs, instead of two, were sometimes observed. At times, even four arcs were also thought to exist; this, however, is relatively uncertain as compared to the observation of three arcs.

Tests were then conducted with the electrical insulators removed and the two nozzle sections brazed together, so that the subsonic and supersonic arcs had a comma negative and the entire nozzle was at the same potential. The operation was satisfactory.

The temperature rise of the various sections, the currents registered, and the visual examination of the electrodes confirmed that the supersonic arc was operating as desired.

A typical mode of operation of the Double Arc unit is illustrated in Fig. 21. In this case, the engine was first operated with a single subsonic arc at 140 amps and 125 volts. Then the supersonic arc was turned on. The supersonic arc circuit had a ballast of 0.25 ohms larger than the ballast in the subsonic arc. When both the arcs were operating the subsonic and the supersonic arcs were drawing currents of 96 and 60 amps respectively, so the total current had increased form 140 to 156 amps. This led to the drop of voltage on the subsonic arc from 125 volts to 90 volts. The voltage across the supersonic arc was 75 volts - the difference between 90 and 75 volts represented the drop in the additional supersonic arc ballast of 0.25 ohms.

Tests were then conducted to determine if it was possible to operate the two arcs at different current and voltage levels and yet have stable arc operation.

The stability criteria of a typical electric arc is shown in Fig. 22(a). The solid line shows the V-I characteristics of an electric arc. The dotted line shows the ballast drop. The points of intersection indicate possible points of arc operation. The upper point gives unstable operation while the lower point gives stable operation.

With the help of appropiate ballast it was possible to operate the subsonic and supersonic arcs at approximately equal currents, as shown by points marked "1" on Fig. 22(b). This, however, necessitates having different potentials at the two pins.

Attempts were then made to determine if the arcs could be operated simultaneously when the current levels in the two discharges were substantially different. A typical operation is shown by points marked "2" on Fig. 22(b).

The solid and the dotted lines in Fig. 22(b) represent the solid and the probable arc discharge and ballast lines at each point, similar to the solid and dotted lines illustrated in detail in Fig. 22(a). Both tests were run at approximately the same total power level - 14.0 KW for the first test and 14.5 KW for the second. The distribution of power between the two arcs was, however, different. In the second case, the subsonic arc had larger power - 9.2 KW for the first test and 12.0 KW for the second test. It was felt that voltage and current for each of the two arcs could be varied, and that a certain amount of control of the two arcs was possible.

Next, the effect of varying the gap in the subsonic arc of a Double Arc unit was determined. The results are shown in Fig. 23. Increasing gap resulted in increase of voltage, current and power level of the subsonic arc. The supersonic arc remained relatively unchanged. The voltage across the supersonic arc increased somewhat, but the current fell, and the power level increased only slightly. The supersonic arc performance was not highly affected by the changes made in the subsonic arc operation.

From the data obtained, it was concluded that it was feasible to operate a subsonic and a supersonic arc simultaneously in a small nozzle. It was also feasible to have variation and control of their individual performance.

Double Arc Characteristics

Test data was correlated, first at constant P to get V-I arc characteristics, and then at constant I to get V-P arc characteristics separately for the subsonic and supersonic arcs.

Data of three tests at approximately 47 psi has been reduced and plotted in Fig. 24. The points belonging to the same test have been paired together by arrows. The V-I characteristics may be represented by $V = A (I)^{-}$. The value of was approximately the same for subsonic and supersonic arcs for the test pressures.

The V-P data has been correlated in Fig. 26 at current levels of 80 amps for the subsonic and 52 amps for the supersonic arc. The plots can be represented by $V = B (P)^m$ where m is 0.4 for the subsonic arc and 0.2 for the supersonic arc. The value for the supersonic case is somewhat uncertain because of the scatter of the test data.

It is noted that the characteristics of the supersonic arc are similar to those expected from a high pressure arc column, rather than a low pressure arc column for which the exponents are smaller.

To be able to compare the arc characteristics with available data, tests were conducted with the subsonic arc only. The V-P data has been shown in Fig. 26 at two current levels, of 60 amps and 150 amps. The V-I data is shown in Fig. 27 for constant pressure level of 50 psia. The V-I data could be represented by $V= (I)^{-n}$, at constant pressure, where $n = 0.8$ at P = 50 psia. The V-P data could be represented by $V = (I)^m$ at constant current. The value of m was 0.7 at 60 amp level and 0.8 at 150 amp level.

Comparing this data for subsonic arc alone with previously available data*, it was found that the exponent for V-I relationship was comparable to the conventional single arc in nitrogen. The exponent for the V-P curves was, however, somewhat higher than previously obtained with nitrogen and copper*. This may be due to the rather strong gas vortex used in the current design.

It therefore appears that the subsonic arc of a Double Arc unit has characteristics substantially similar to that of a single arc engine. The supersonic arc characteristics are somewhat similar although the exponent in the $V = (P)^m$ relationship appear to be somewhat smaller than for the subsonic arc.

---

*"Gaseous Conductors", J.D. Cobine, Dover Publication, 1957, Pages 296 and 297.

Gas Enthalpy

The gas enthalpy at the exit of the unit was computed by the energy balance method, by measuring the electrical input to the engine and the thermal losses from the engine. The gas enthalpy varied about 10,000 to 32,000 Btu/lb.

It is of interest to note that gas enthalpy values up to 32,000 Btu per lb were measured. Comparison with available data indicates that these enthalpy levels are considerably higher than the values obtained in the past. For instance, the maximum total enthalpy that has ever been achieved previously with nitrogen is on the order of 15,000 Btu per lb at 3.5 atm pressure*.

The number of test points presently available at very high enthalpy levels are too few to make firm conclusions concerning the magnitude of increase; this is expected to be done when larger number of tests at high enthalpy levels are available. The attainment of higher enthalpies would give an indirect proof of the ability to accomplish higher specific impulse.

Heat Flux

As indicated earlier, the purpose of segmenting the nozzle was to ascertain the locations of arc attachment, and determine the distribution of heat transfer in a nozzle with supersonic heating. The nozzle had three segments - the nozzle throat section (also called the subsonic nozzle electrode), the supersonic arc nozzle electrode segment, and the after-expansion nozzle segment (also called the nozzle skirt). The heat transfer to these three segments, as well as to the subsonic arc pin electrode and the supersonic arc pin electrode, was measured separately by noting the temperature rise and the flow rate of the coolant through each segment.

It was noted that heat transfer to the supersonic nozzle electrode segment was larger than the heat transfer to the after-expansion nozzle segment, indicating the supersonic arc attached in the section immediately after the throat and not at the end of the nozzle. This indicated the feasibility of adding energy immediately after the throat and having an after-expansion. It would not be desirable to add energy near the end of the nozzle, where there would be no after-expansion.

To be able to compare the heat transfer to various components with the case of a single arc only, attempts were made to run tests under identical operating conditions. The propellant flow, and the total power level into the engine were kept approximately the same. The results have been given in Table 3.4 and Fig. 28. The table gives the direct experimental data; however, in Fig. 28, data of single arc has been reduced to the same power level as of Double Arc to enable comparison under comparable conditions.

---

*Arnold Engineering Development Center, TDR 62-145, Tullahoma, Tennessee

Table 4 Effect of Double Arc Operation on Heat Transfer to Different Components

Item	Subsonic Arc Only	Subsonic and Supersonic Arcs
Operating Conditions		
Propellant Flow, lbs/sec x 10^{-3}	0.44	0.44
Power Input, Subsonic KW	12.48	7.98
Supersonic KW	--	4.16
Total	12.48	12.14
Chamber Pressure, psia	27.2	24.7
Heat Transfer, Btu/sec		
Nozzle Throat section	1.95	0.98
Nozzle Supersonic Arc Section	0.29	0.82
Nozzle After Expansion Section	0.48	0.66
Pin Electrode, Subsonic	1.42	0.90
Pin Electrode, Supersonic	2.20	2.60

The data shows that the use of Double Arc diminished the heat transfer at the critical location of the nozzle throat section. The heat transfer to the nozzle immediately after the throat increased. The heat transfer in the after-expansion part of the nozzle also increased slightly. These measurements confirmed the fact that the energy addition to the nozzle could be as postulated in the concept.

Also, the heat transfer to the subsonic electrode was significantly reduced when the unit was operated as a Double Arc. Heat transfer to supersonic pin electrode increased with the presence of the Double Arc. The increase was, however, small (about 20%) indicating that most of the heat transfer to the pin was by convection rather than by arc attachment.

It should be noted that while operating the unit as a single arc, it was necessary to keep the supersonic pin electrode inside the unit, although it carried no power. This was necessary for maintaining the same throat area so that the comparison could be made under approximately identical conditions. If the supersonic pin electrode had been removed, the unit would have had a much larger nozzle throat area for the single arc case than for the Double Arc case.

Since the heat transfer to various components as well as the power input to the two arcs was measured, it is possible to calculate the energy transferred to the propellant at various locations along the length of the nozzle. This has been calculated in the Table 5, using the test data given previously in Table 4, and plotted in Fig. 29. This illustrates the achievement of the energy transfer as postulated for the Double Arc. It also shows that for engines operating at the same total power input, energy level at the throat is lower for the Double Arc.

Tests to check the Double Arc feasibility and compare operation with single arc, were repeated at three pressure levels. Results were substantially similar to those shown for 25 psia before. In case of the 45 psia tests, the percentage of total power introduced in the supersonic arc was increased from 34 to 41 percent. The results are shown in Figs. 30 and 31.

Table 5 Effect of Double Arc Operation on Energy Transfer to the Propellant at Various Locations in the Nozzle

Item	Subsonic Arc Only	Subsonic and Supersonic Arc
Operating Conditions		
Propellant Flow, lbs/sec x 10^{-3}	0.44	0.44
Power Input, Subsonic KW	12.48	7.98
Supersonic, KW	--	4.16
Total	12.48	12.14
Chamber Pressure, psia	27.2	24.7
Energy Input		
Subsonic Arc Addition	11.80	7.55
Less Subsonic Pin Electrode	10.38	6.65
Less Nozzle Throat Section	8.43	5.67
Plus Supersonic Arc Addition	--	9.62
Less Supersonic Pin Electrode	6.23	7.02
Less Supersonic Arc Nozzle Section	5.94	6.04
Less Nozzle After Expansion Section	5.46	5.38

Nature of Supersonic Arc Attachment

Some observations concerning the nature of attachment of the supersonic arc, are noteworthy.

The examination of the electrode surfaces indicated that the subsonic arc left the familiar tracks of arc "spots" on both the subsonic pin electrode and the subsonic nozzle electrode. Similar tracks were not present on the supersonic pin electrode or the supersonic nozzle electrode; indicating that the supersonic arc column did not attach on a small "spot" with high current density but perhaps as a "sheath" with low current density, or perhaps as a spot with such large diameter and low current density that it left no marking on the electrode surface.

The "sheath" type of discharge has lower current density for the same current. The lower current density may be expected to result in lower heat transfer to the electrode. This may be responsible for the rather small increase in heat transfer noticed during the tests, both to the supersonic pin electrode and the supersonic nozzle electrode.

Sheath discharge would have other advantages. It would tend to heat the gas more uniformly than the column discharge which represents a high temperature core surrounded by gas at lower temperatures. It would also result in a more stable operation than a moving column discharge. This might explain the high stability of the supersonic discharge noted.

Several factors point to the presence of a sheath discharge, except that the V-I and the V-P characteristics of the supersonic arc were found to be similar to those of a column discharge. It is expected that availability of additional data in future might result in clarification of the nature of the discharge.

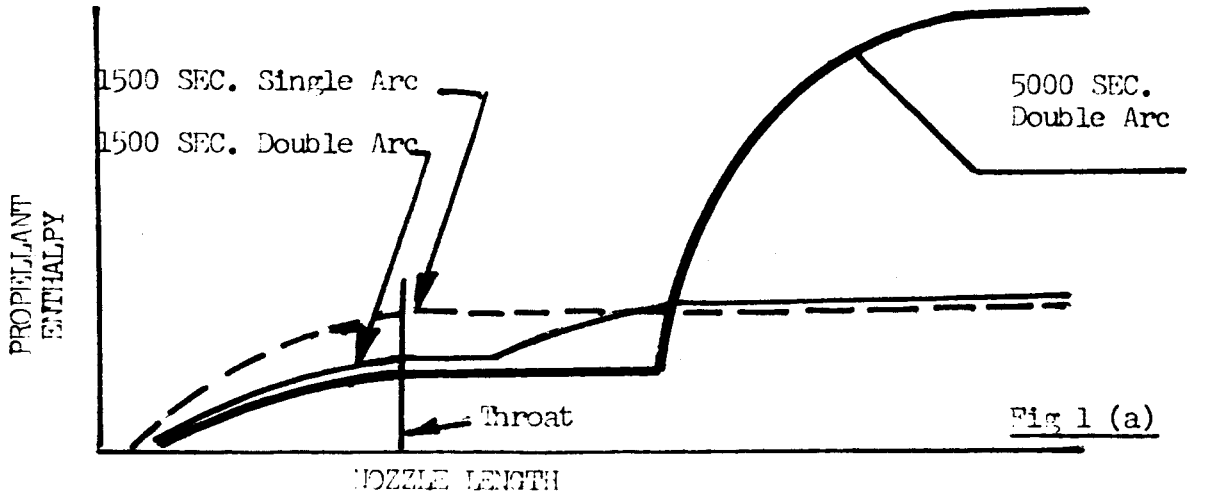

Fig 1 (a)

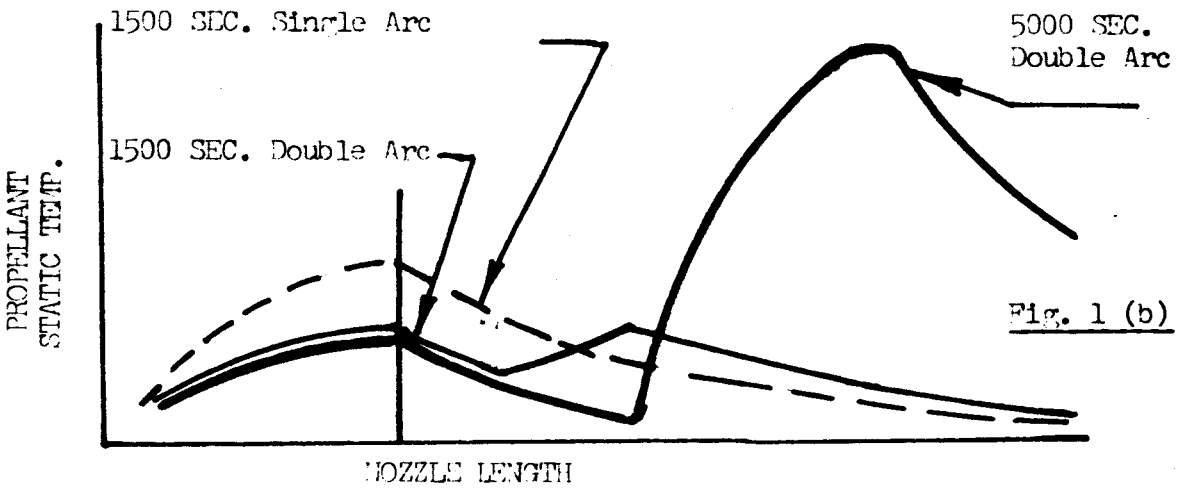

Fig. 1 (b)

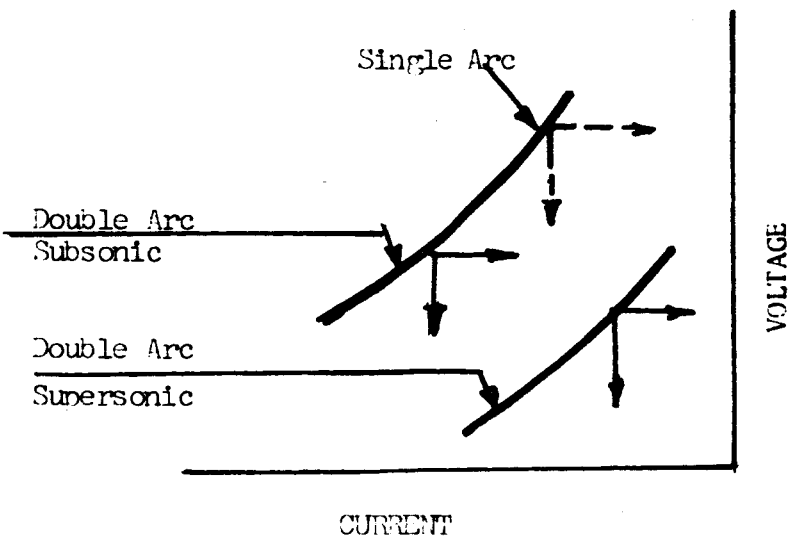

Fig. 1 (c)

Fig. 1 Schematic Performance of Double Discharge Engine

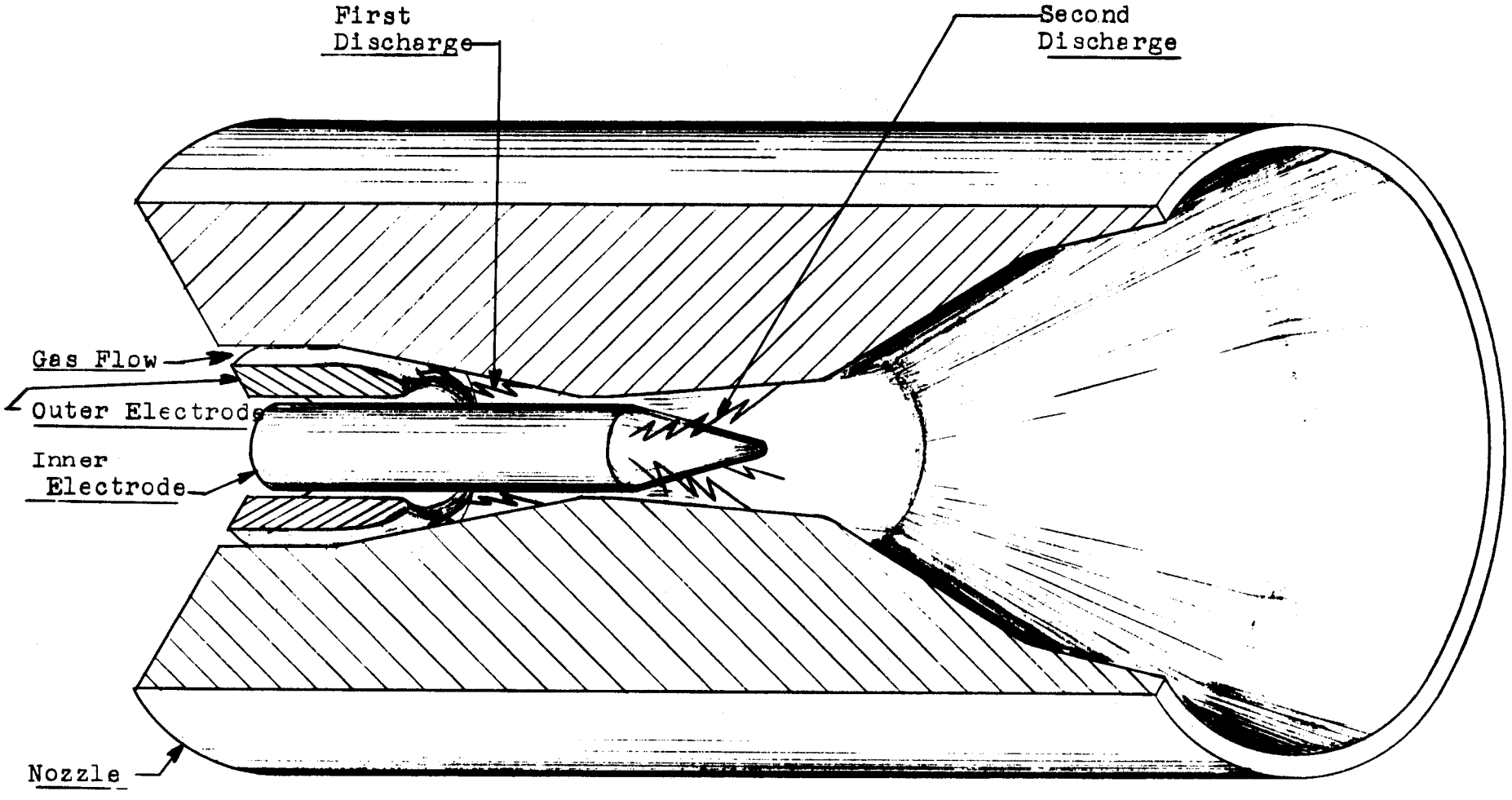

Fig. 2 DOUBLE ARC CONCEPT Proprietary

Plasmajet Systems Division
Space Dynamics Corp.

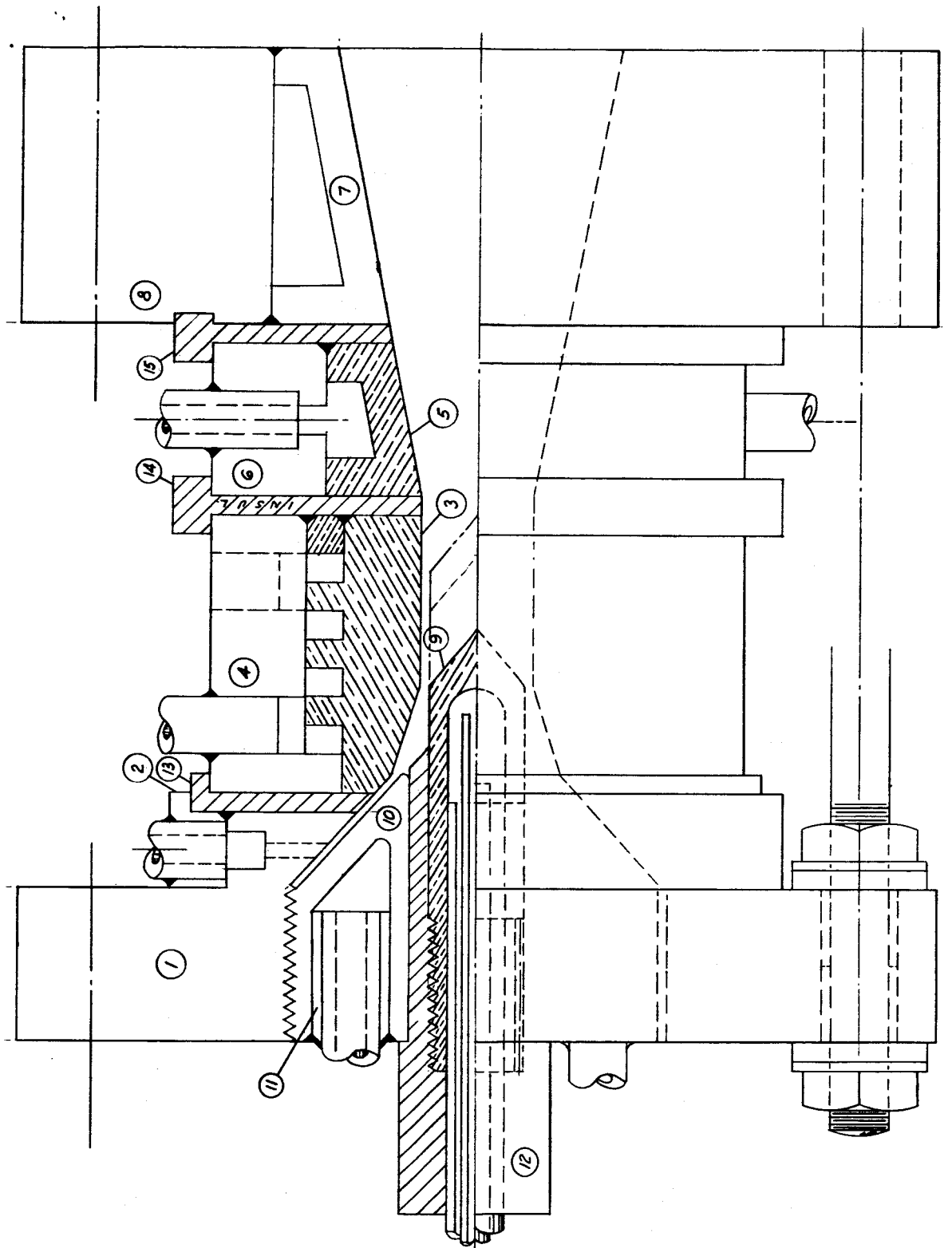

SPACE DYNAMICS CORP.

PLASMAJET SYSTEMS

DOUBLE ARC ENGINE

REVISIONS			
NO.	DATE	BY	
1			
2			
3			
4			
5			

DRAWN BY S.P. | SCALE 4 X | MATERIAL

CHK'D H.K. | DATE July 62 | DRAWING NO. SDC-03-301

TRACED | APP'D N.P. - M.G.

Fig. 3

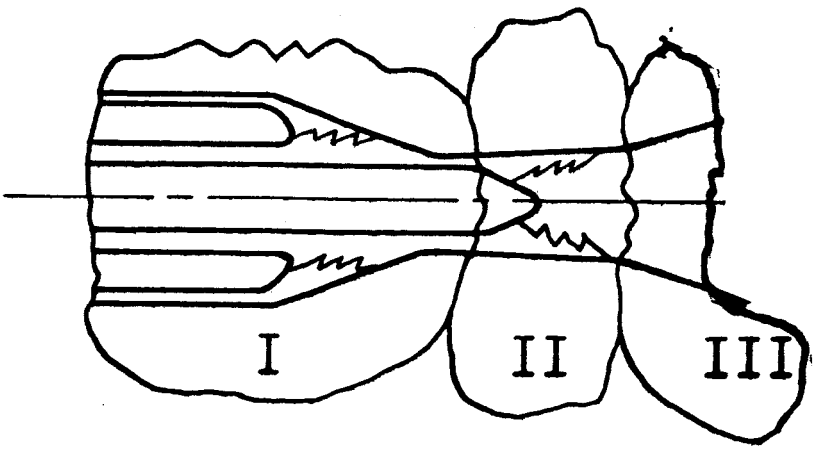

Fig. 4 THREE REGIONS OF DOUBLE ARC ENGINE

I Subsonic Arc and Expansion to Sonic Velocity, (0-1-3)

II Supersonic Arc and Simultaneous Expansion, (3-4)

III Expansion, (4-5)

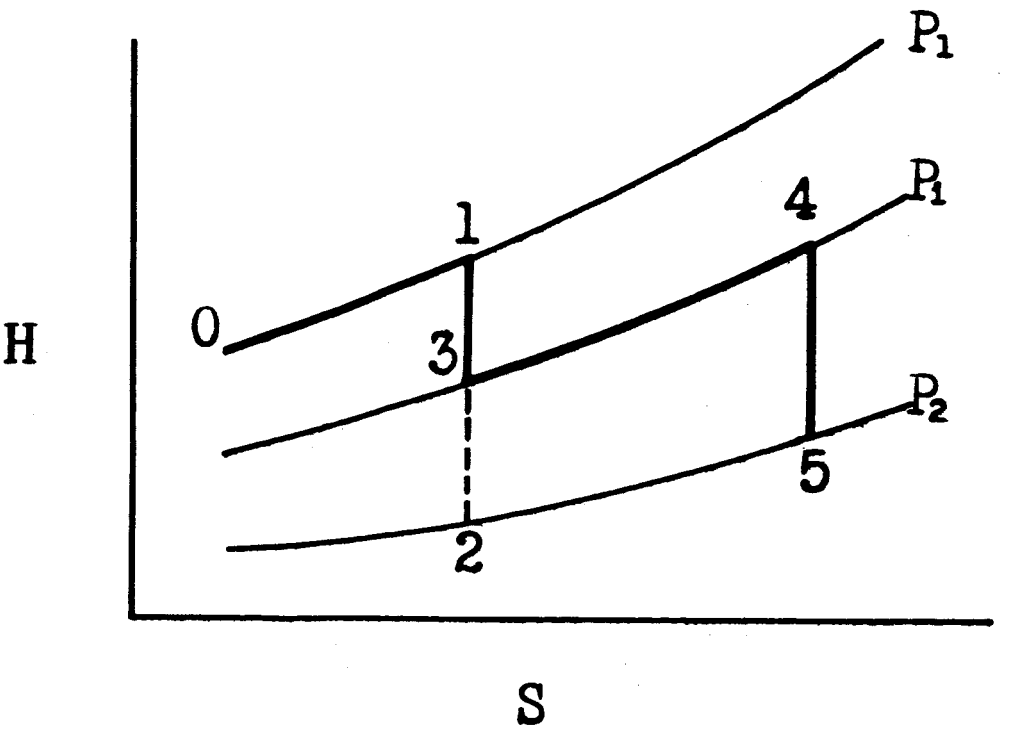

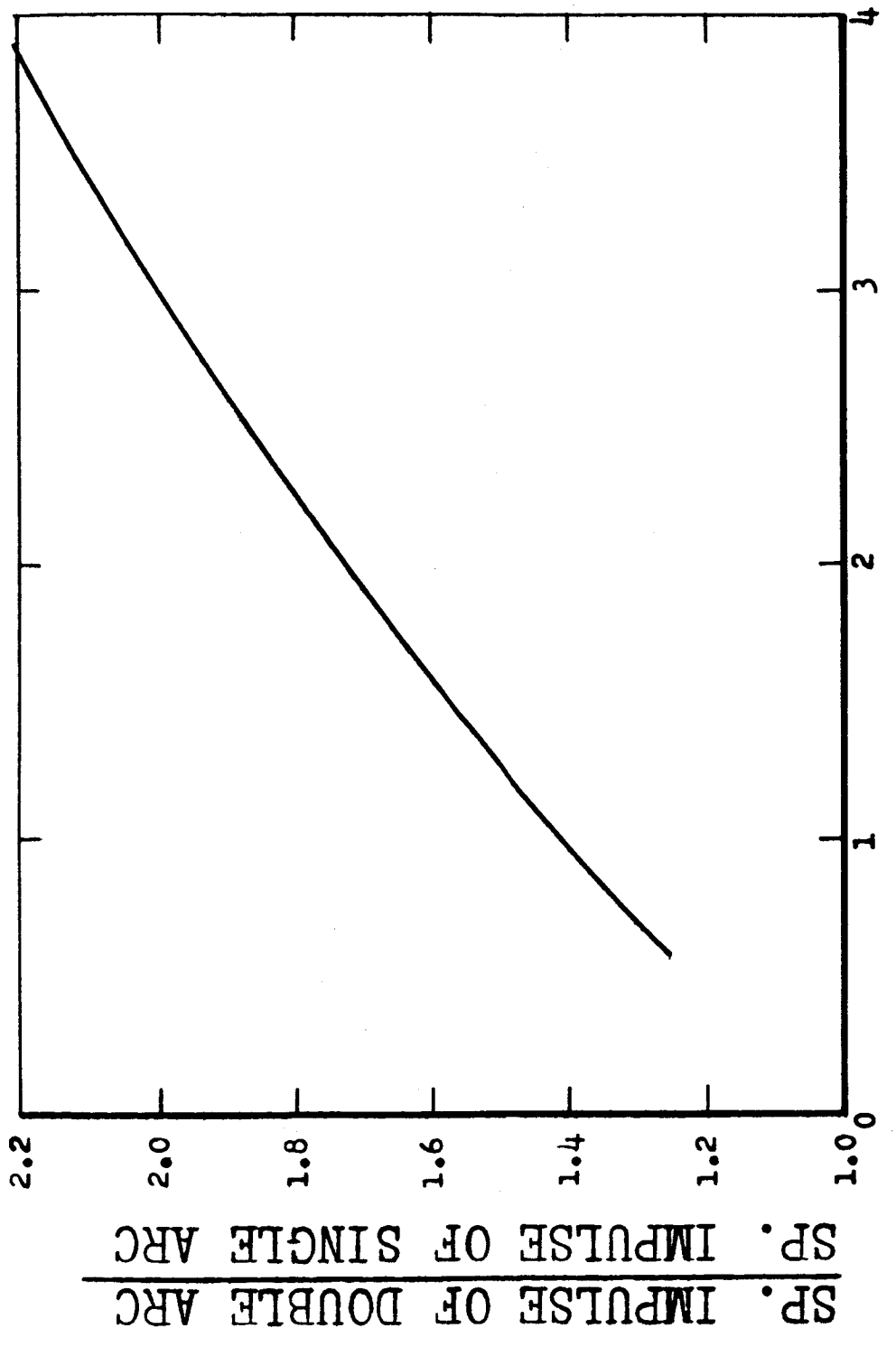

Fig. 5 Theoretical Specific Impulse Increase versus Reheat Temperature Ratio, with no dissociation or ionization.

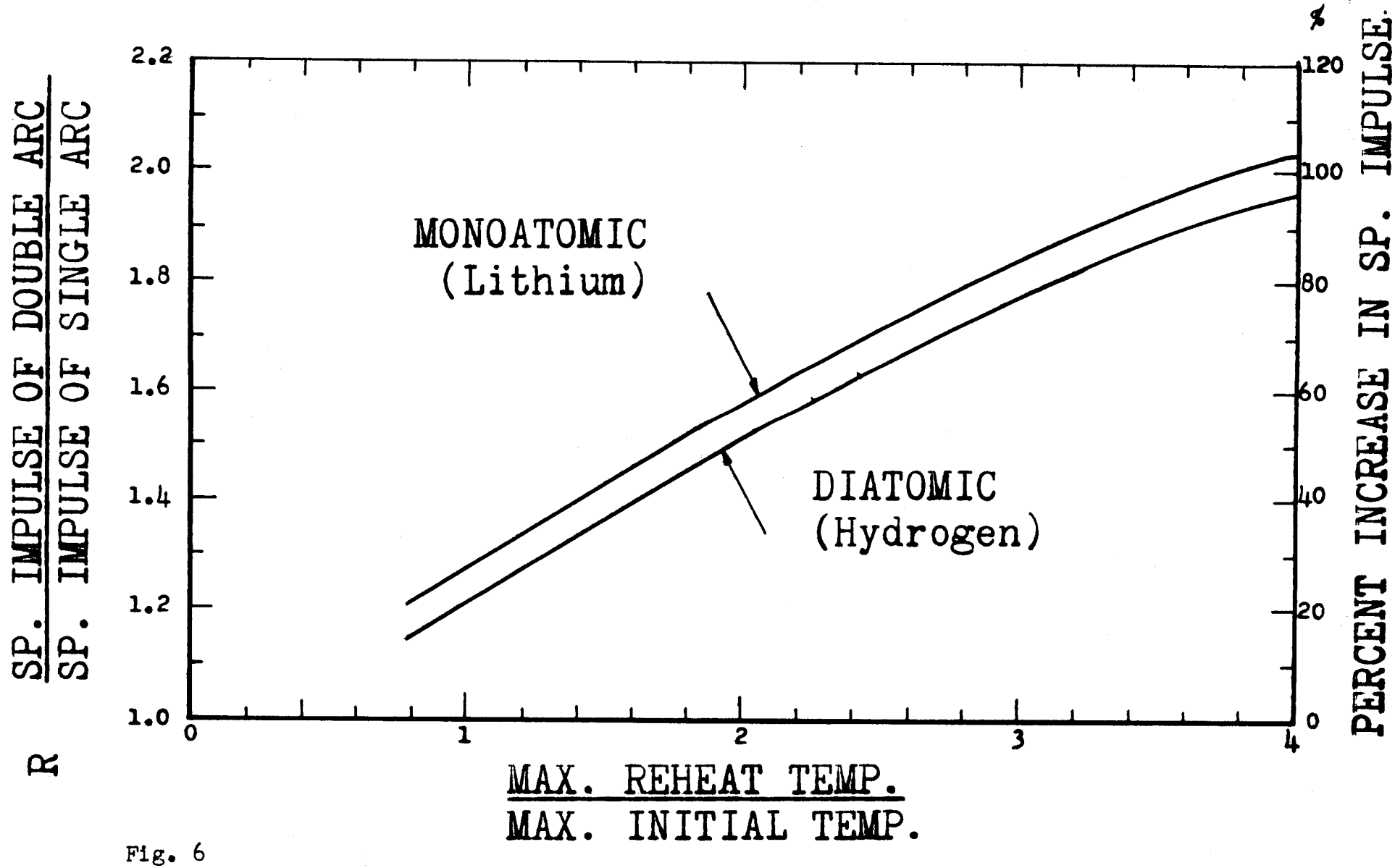

Fig. 6

Theoretical Specific Impulse Increase versus Reheat Temperature Ratio, for Nozzle Expansion Ratio of 1000.

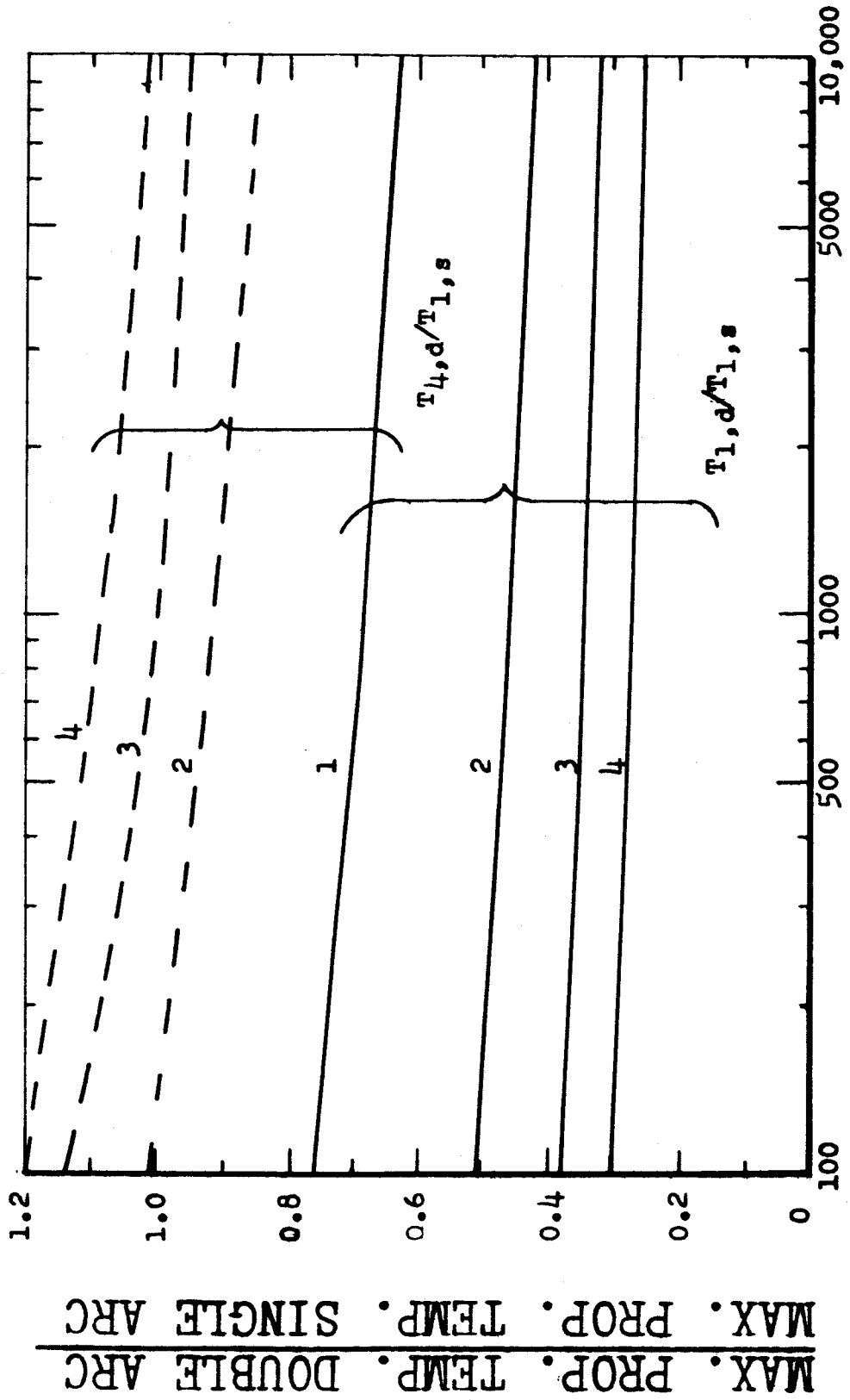

Fig. 7 Reduction of Maximum Propellent Temperature as a Function of Reheat Temperature Ratio, β, and expansion Ratio. $T_{1,s}$ is the Maximum Temperature for Single Arc. $T_{1,d}$ and $T_{4,d}$ are maximum Temperatures for the Double Arc in Subsonic Region (Point 1) and Supersonic Region (Point 4) respectively, Operating at Same Specific Impulse as Single Arc Engine. This is for an Ideal Monoatomic Propellent.

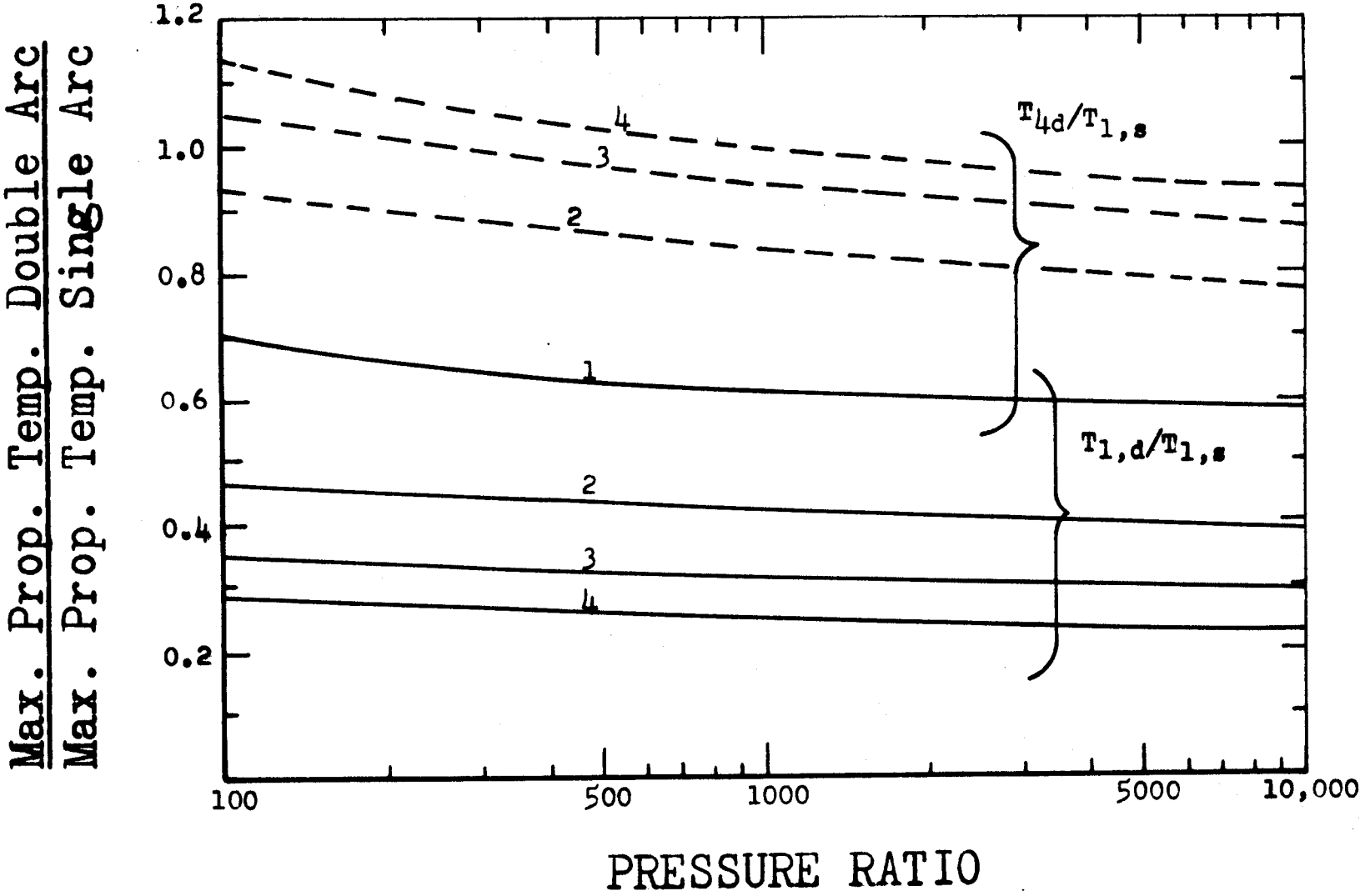

Fig. 8 Reduction of Maximum Propellant Temperature as a Function of Reheat Temperature Ratio, β and Expansion Ratio. $T_{1,s}$ is the Maximum Temperature for Single Arc. $T_{1,d}$ and $T_{4,d}$ are Maximum Temperatures for the Double Arc in Subsonic Region (Point 1) and Supersonic Region (Point 4) Respectively, Operating at Same Specific Impulse as Single Arc Engine. This is for an Ideal Diatomic Propellant.

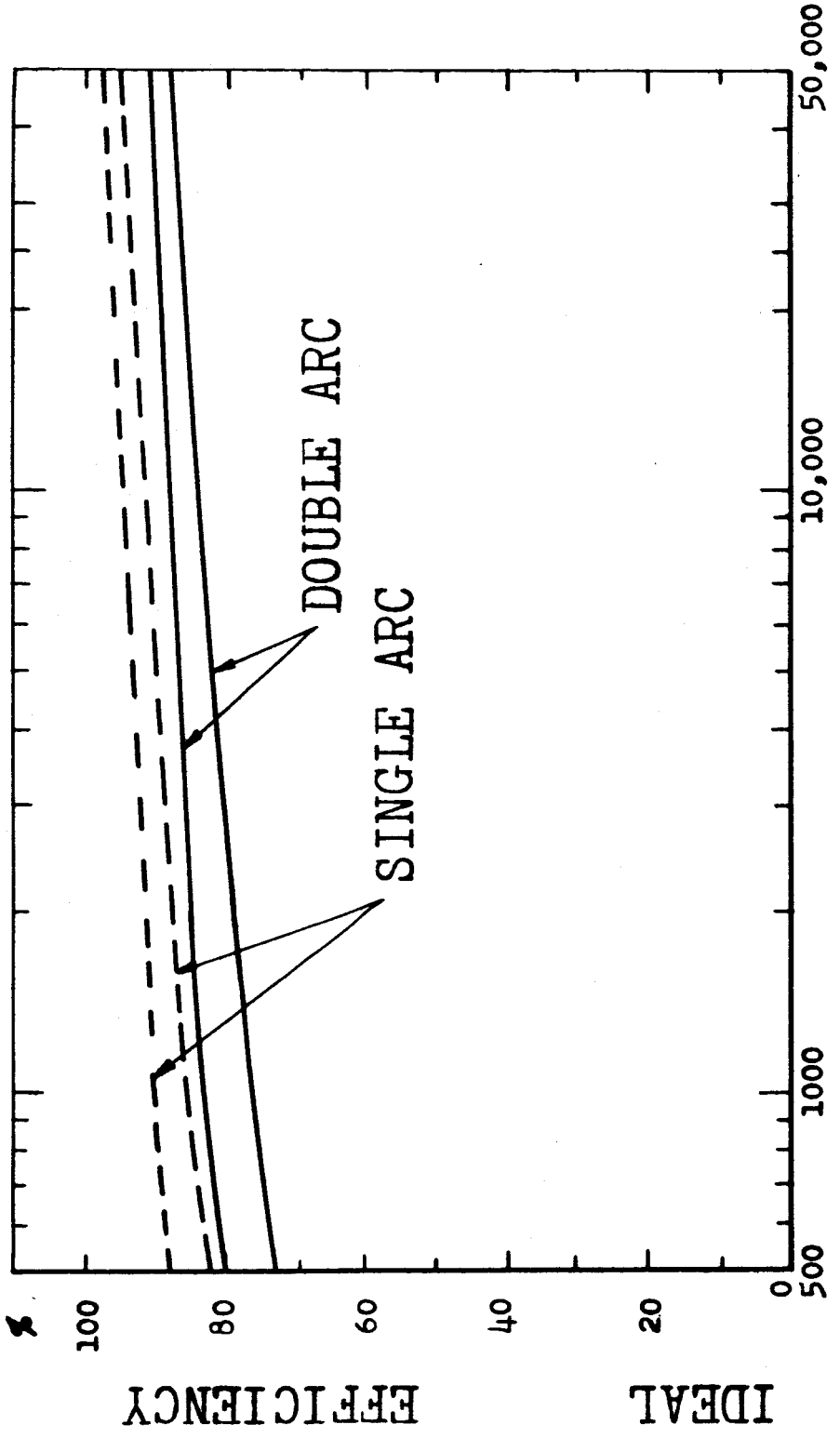

Fig. 9

Theoretical Expansion Efficiency versus Overall Pressure Ratio. Higher Curves for Double Arc and Single Arc Include Allowance for Additional Thrust Due to Exit Pressure.

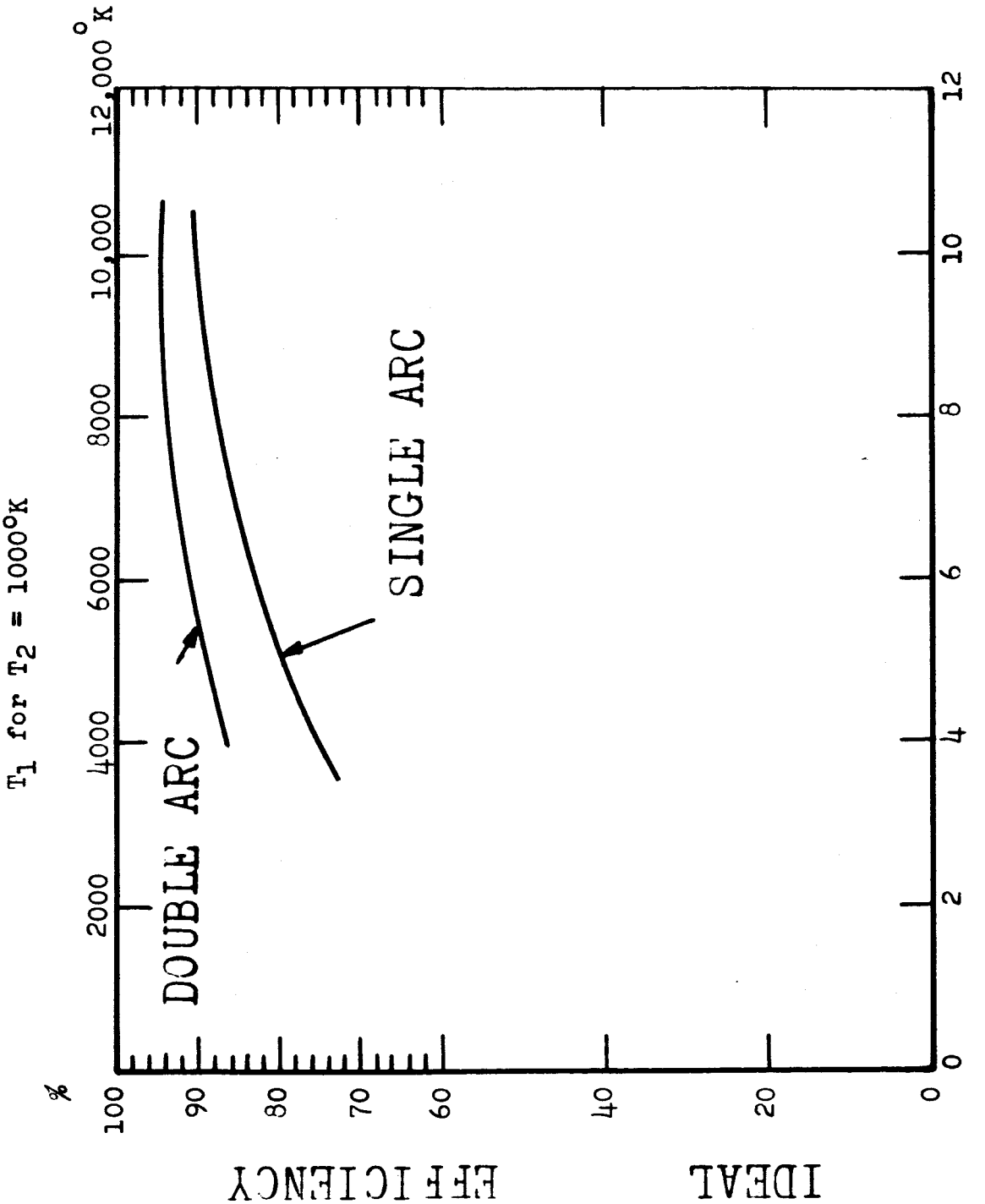

Fig. 10 Theoretical Expansion Efficiency versus Temperature Ratio

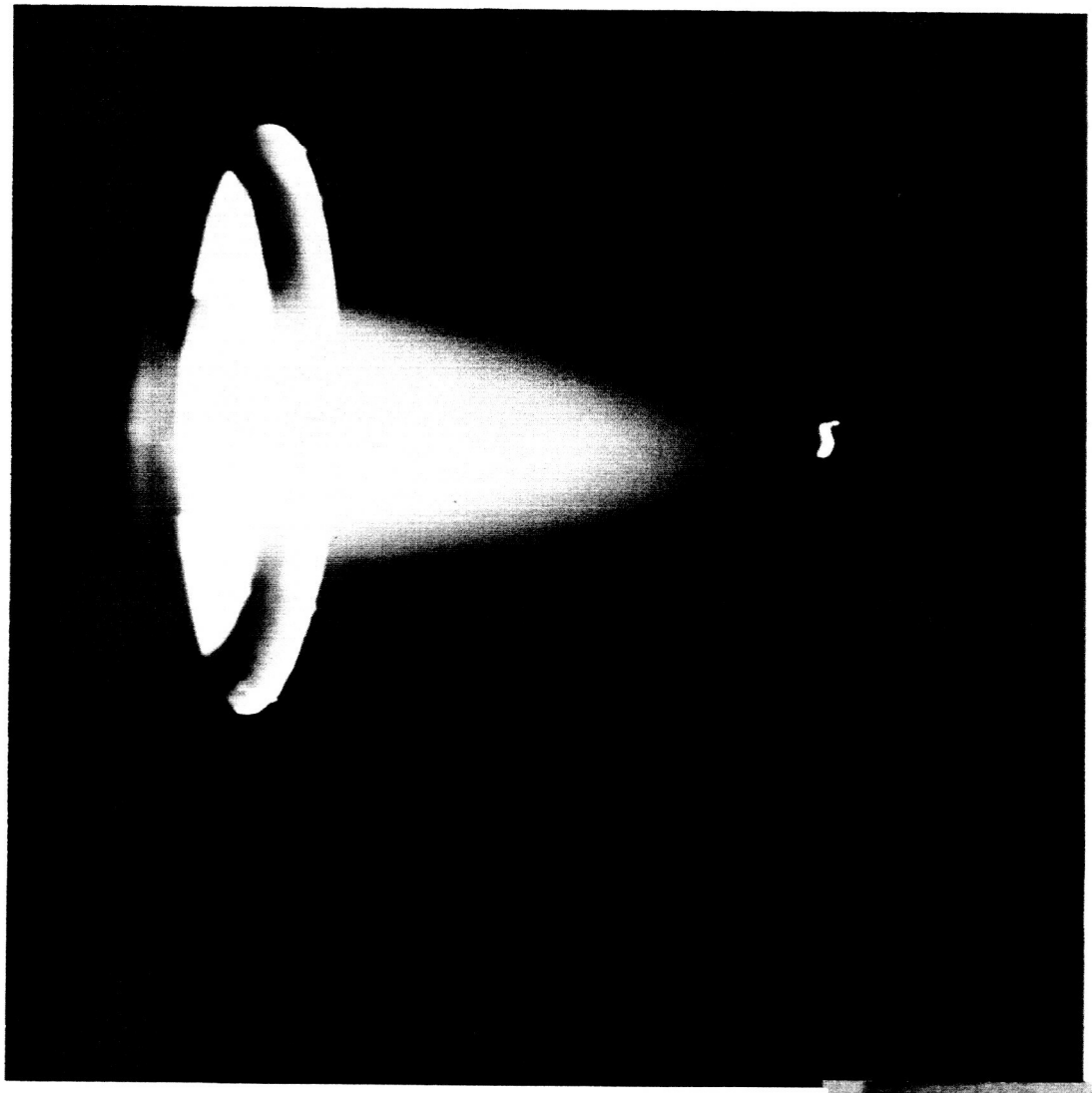

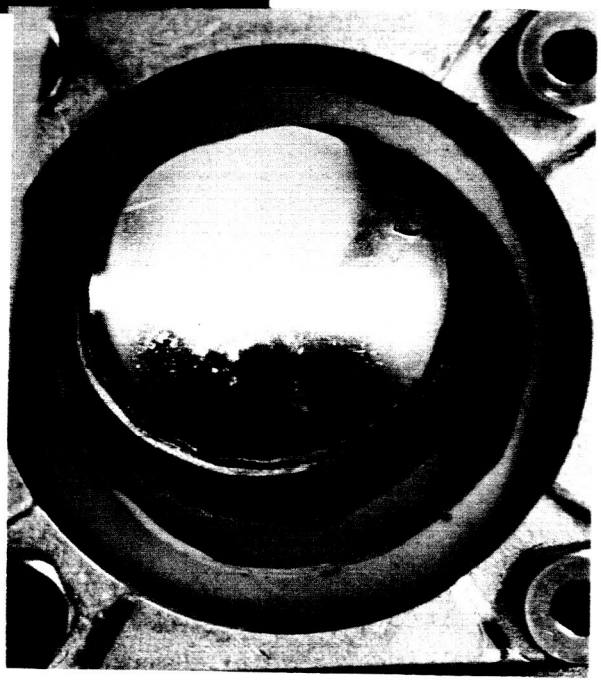

Fig. 11 (Top) High Pressure arc plasma jet exhausting at atmospheric pressure.

(Right) Subatmospheric discharge viewed through a window.

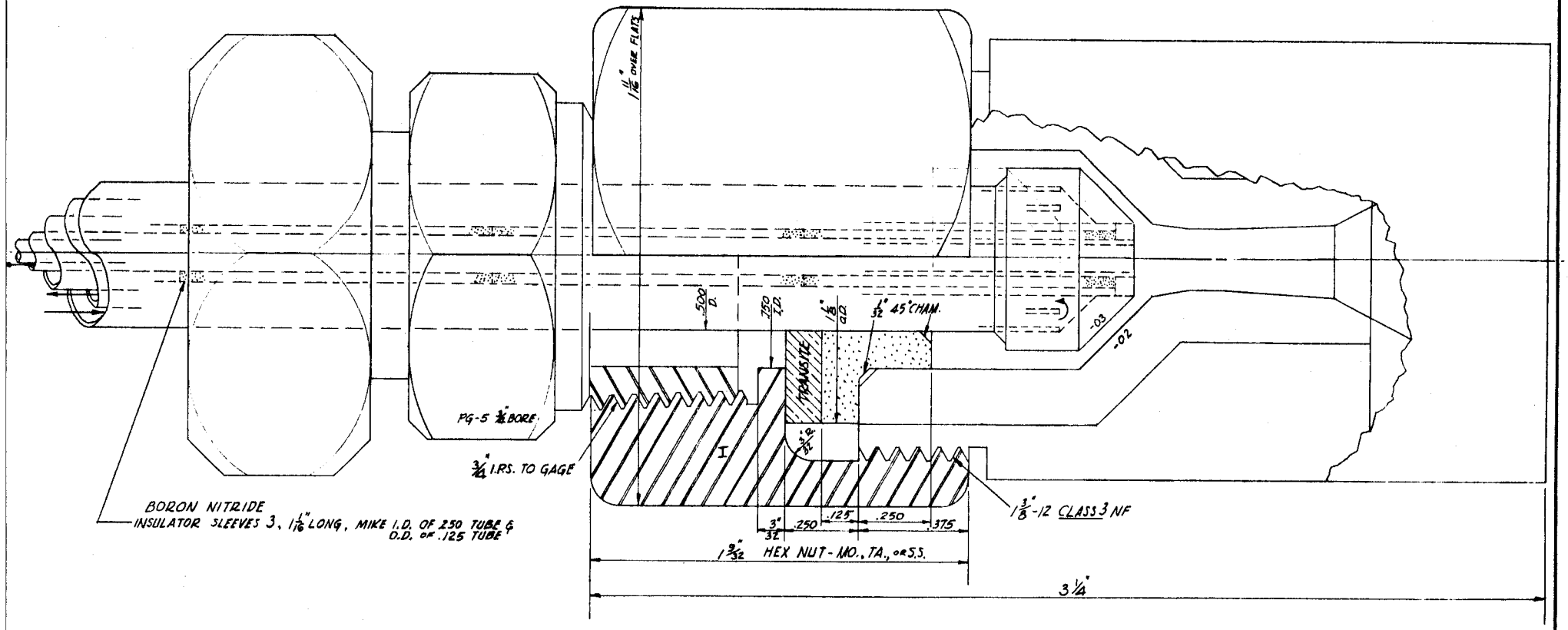

Fig. 12

REVISIONS			SPACE DYNAMICS CORP.
NO.	DATE	BY	PLASMAJET SYSTEMS
1			END ASS'Y.
2			
3			DRAWN BY S.P. SCALE 4x MATERIAL
4			CHK'D H.K DATE 4/25/62 DRAWING NO. SDC-03-2-05
5			TRACED APP'D N.P

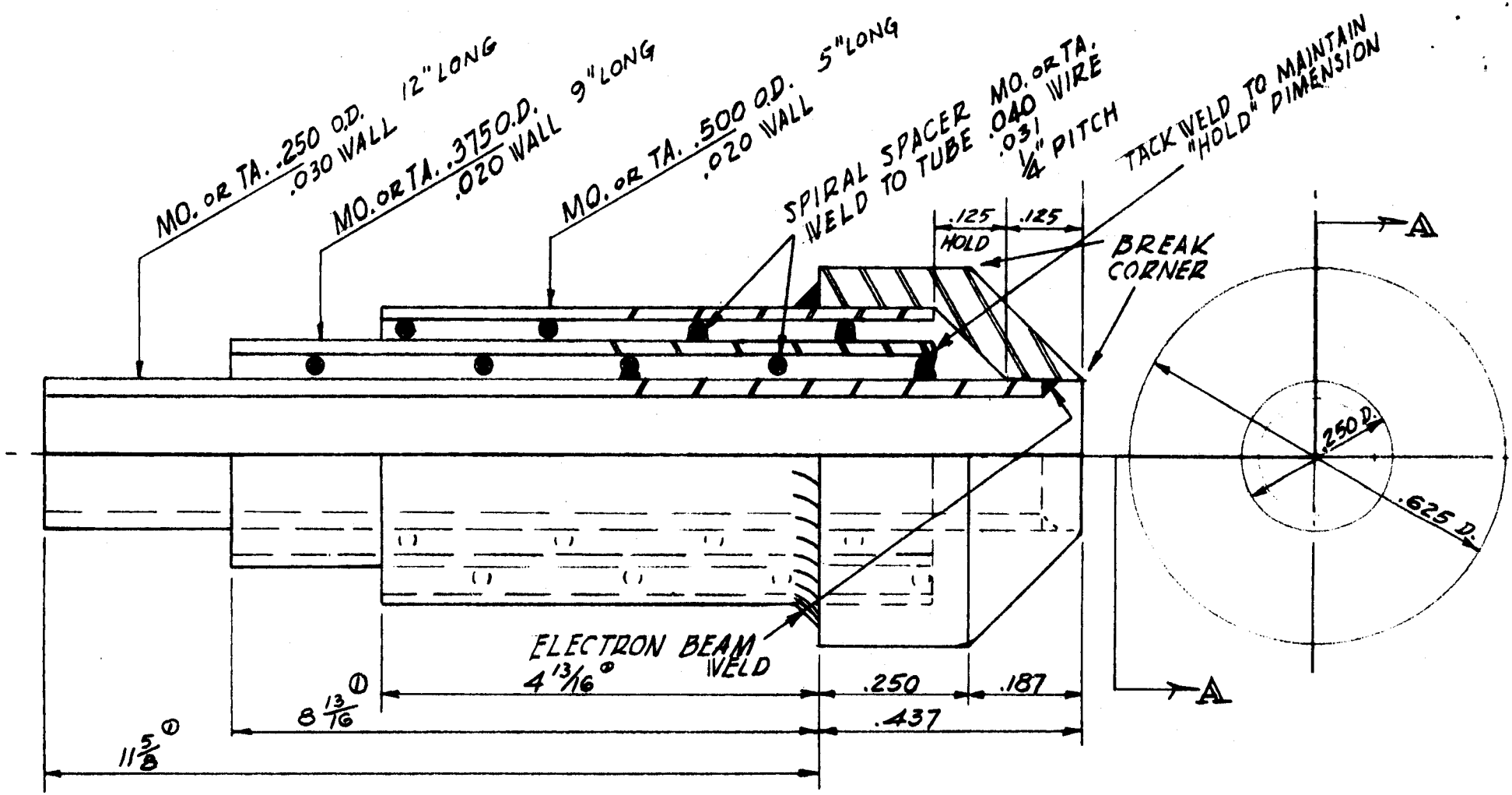

Fig. 13

SPACE DYNAMICS CORP.

REVISIONS		
NO.	DATE	BY
1	4/25/62	
2		
3		
4		
5		

PLASMAJET SYSTEMS →

OUTER ELECTRODE ASS'Y.

DRAWN BY SP	SCALE 4x	MATERIAL
CHK'D HK	DATE 3/30/62	DRAWING NO. SDC-03-2-03
TRACED	APP'D HK	

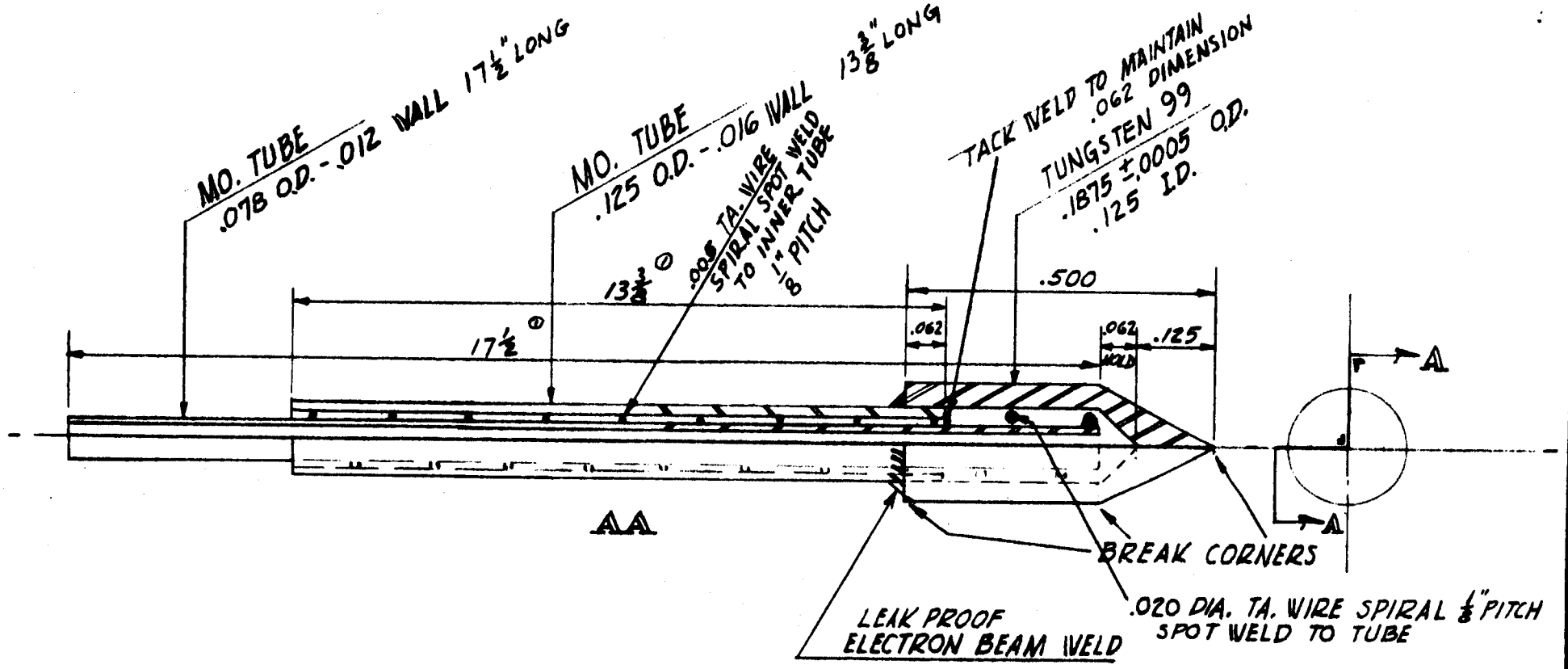

Fig. 14

SPACE DYNAMICS CORP.

REVISIONS		
NO.	DATE	BY
1	4/25/62	
2		
3		
4		
5		

PLASMAJET SYSTEMS

INNER ELECTRODE ASSY.

DRAWN BY SP	SCALE 4 x	MATERIAL
CHK'D HK	DATE 3/30/62	DRAWING NO. SDC-03-2-04
TRACED	APP'D HK	

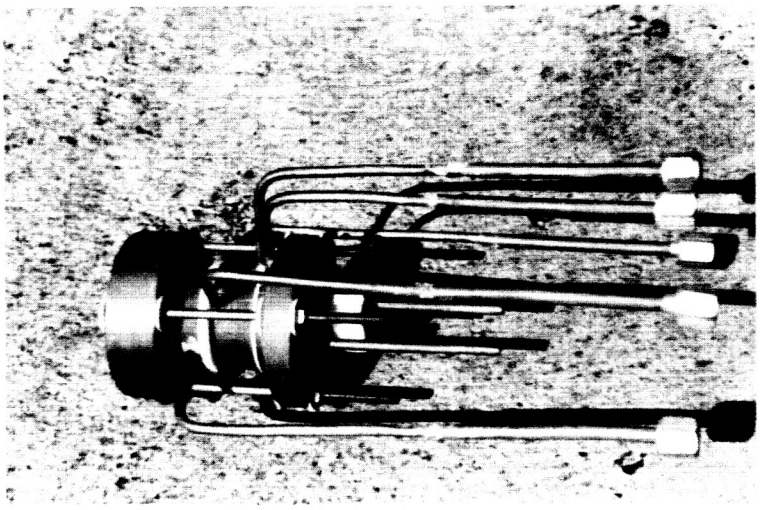

Double Arc Research Model - The nozzle is segmented to measure energy transfer to different parts of the nozzle separately. Energy transfer to the electrodes is also measured separately.

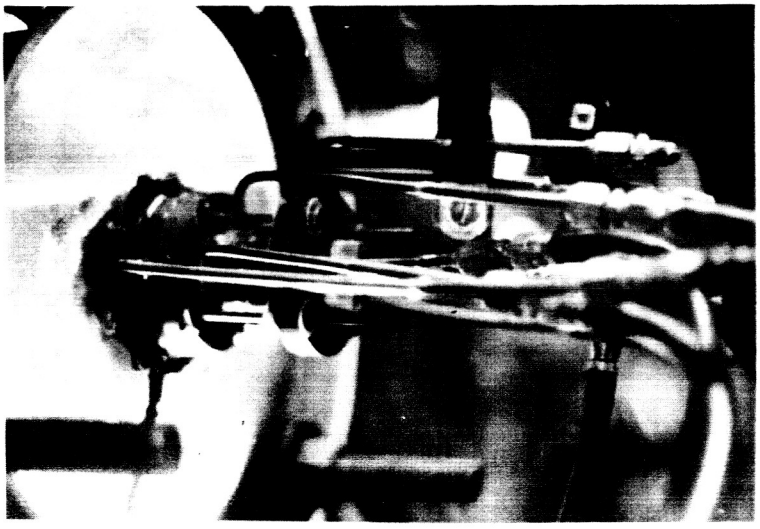

Research Unit installed in Vacuum Tank.

Fig. 15

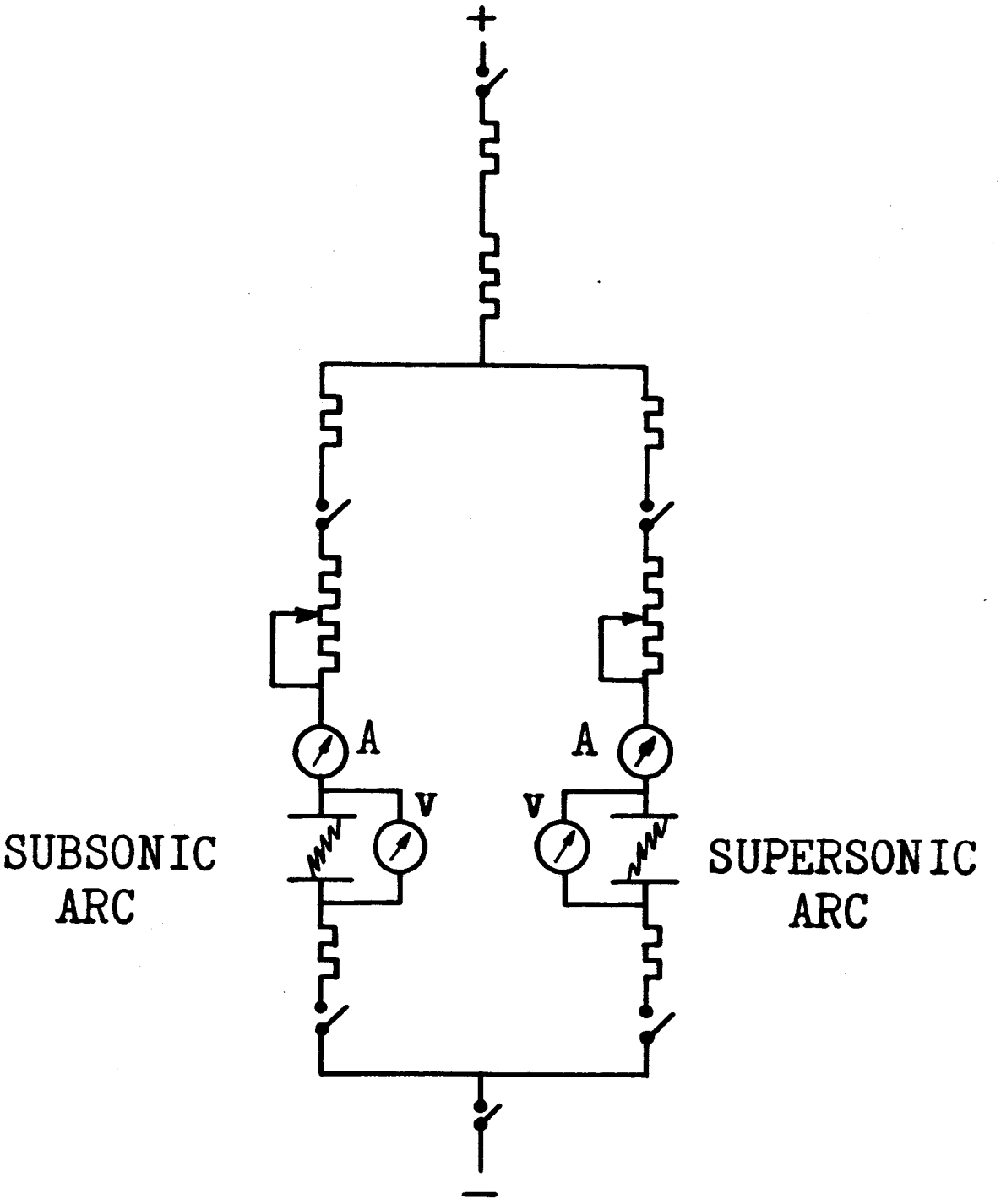

Fig. 16 Schematic of Electrical Test Set Up

LABORATORY FACILITIES

Fig. 17 Facilities for Research and Testing at S. D. C. Laboratory -- (Top Left) Six vernier rheostats for providing control of several electrical circuits with large current carrying capacities; (Top Right) Console for control and regulation of cryogenic fluids; (Bottom Left) Master Flow Control Console for large gas flows at pressures up to 3000 psi; (Bottom Right) Bank of arc ballasts capable of currents up to 5000 amps.

TEST SET UP

Fig. 18 A Typical Test Set Up

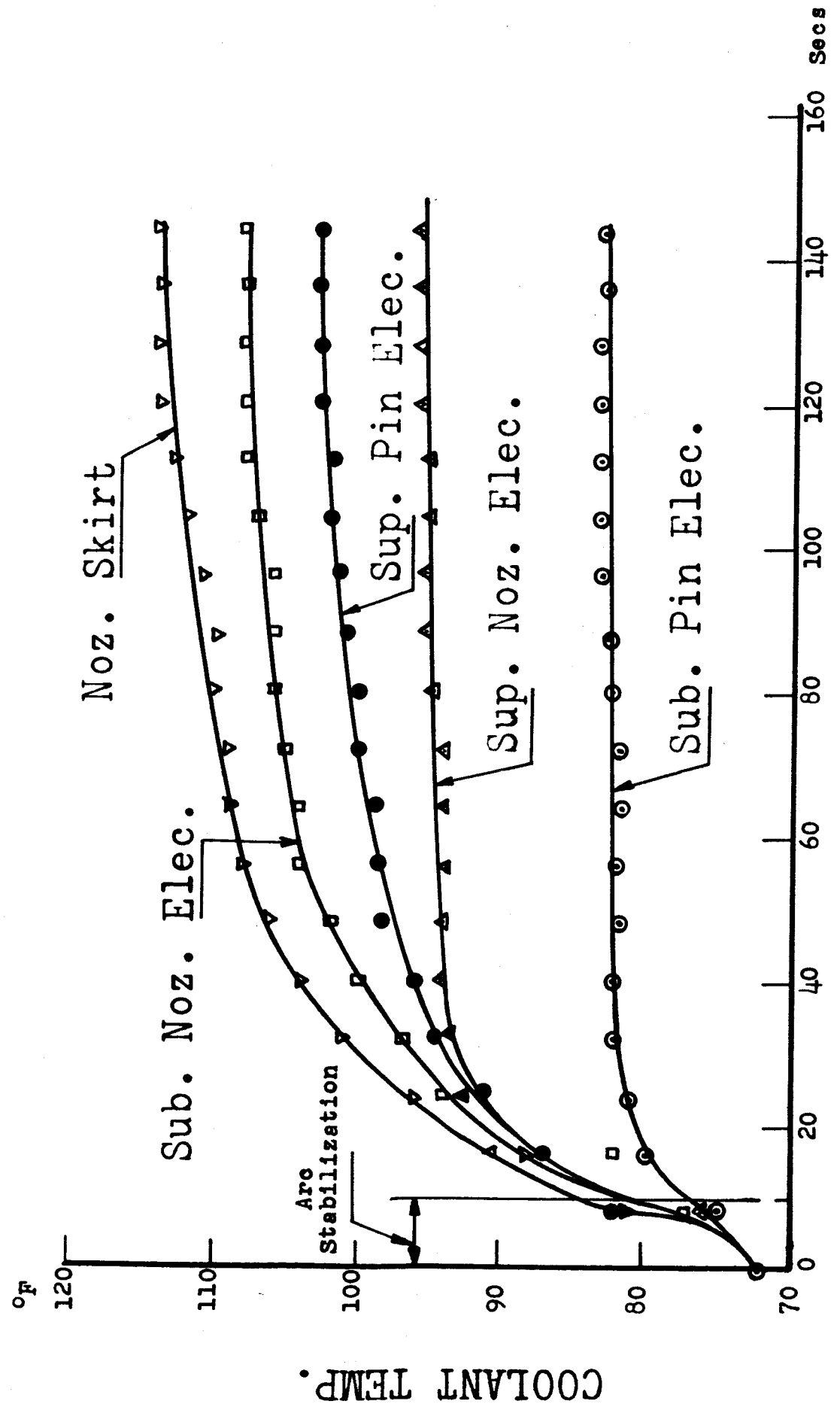

Fig. 19 Typical Variation of Coolant Temperature at Exit from Engine

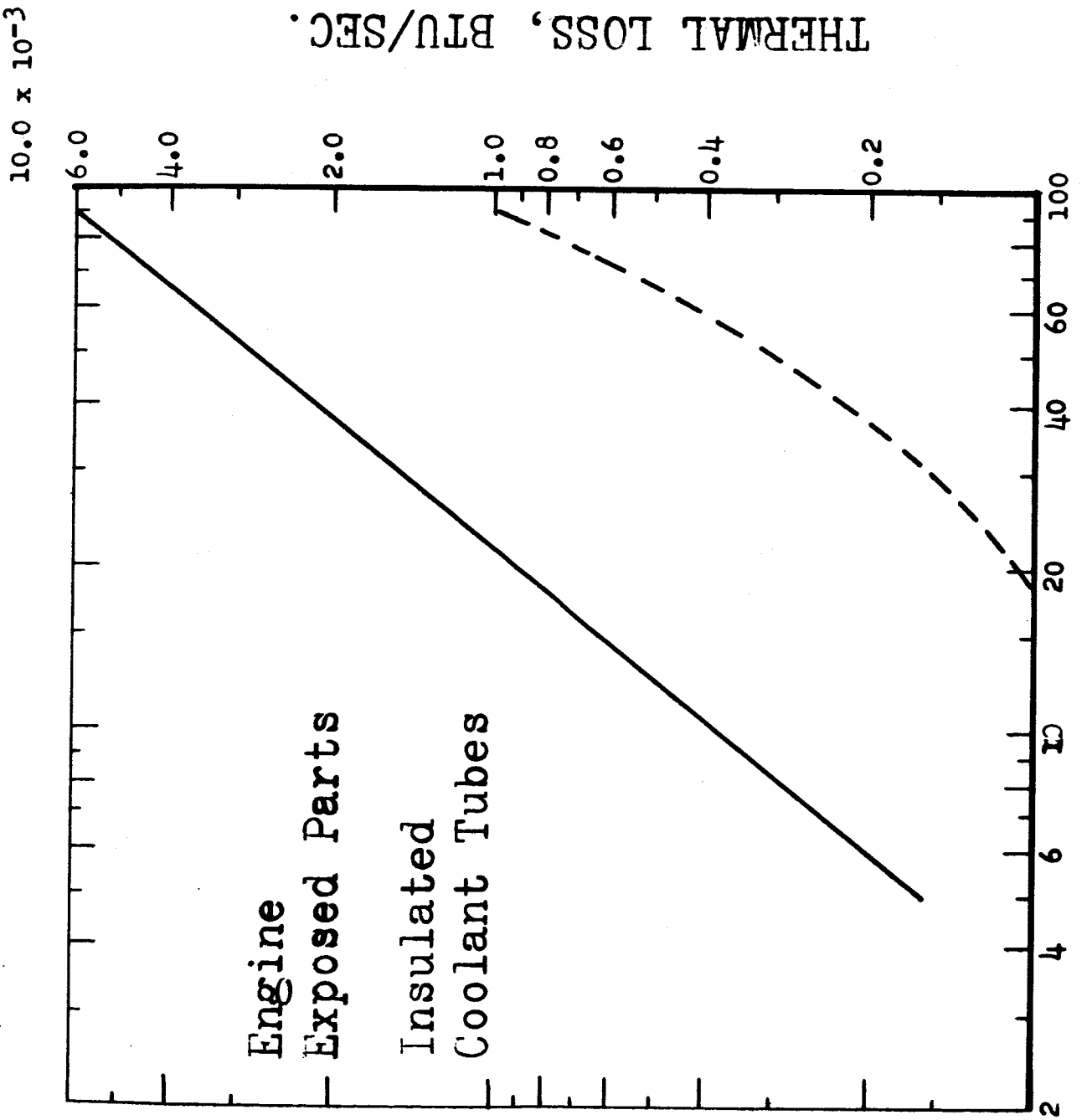

Fig. 20 Thermal Loss Characteristics of the Test Apparatus

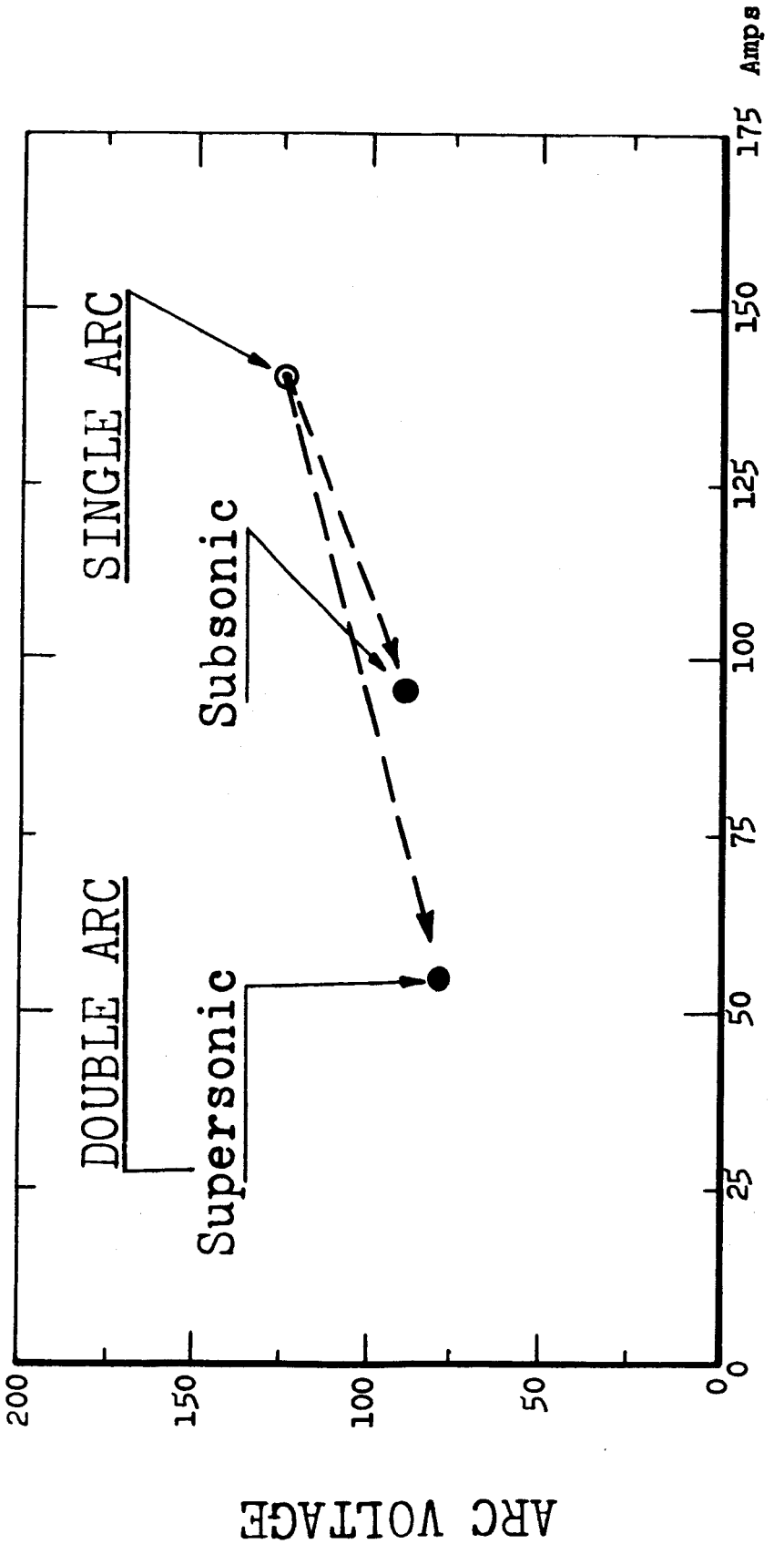

Fig. 21 Typical Transfer from Single Arc Operation to Stable Double Arc Operation

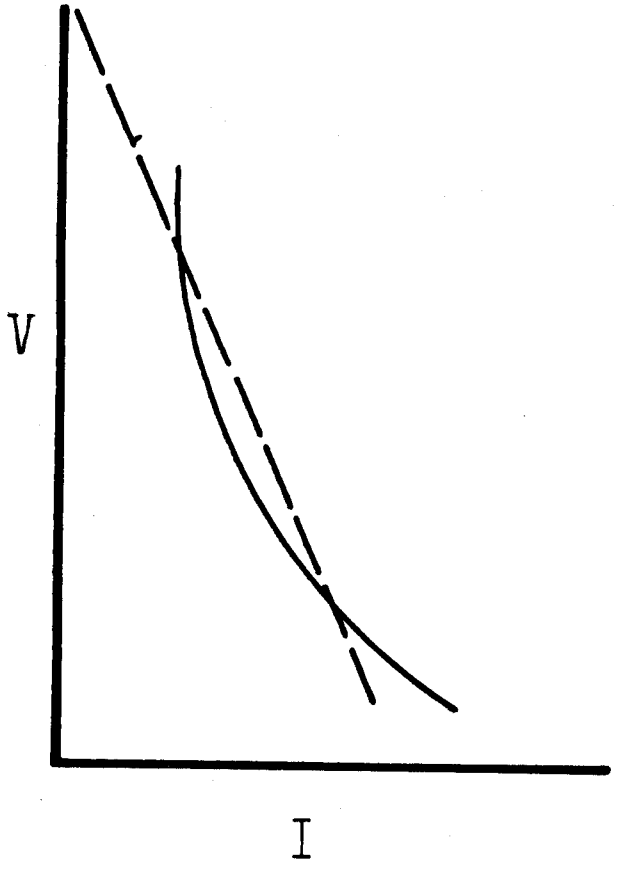

(a) Stability Criteria of an Electric Arc

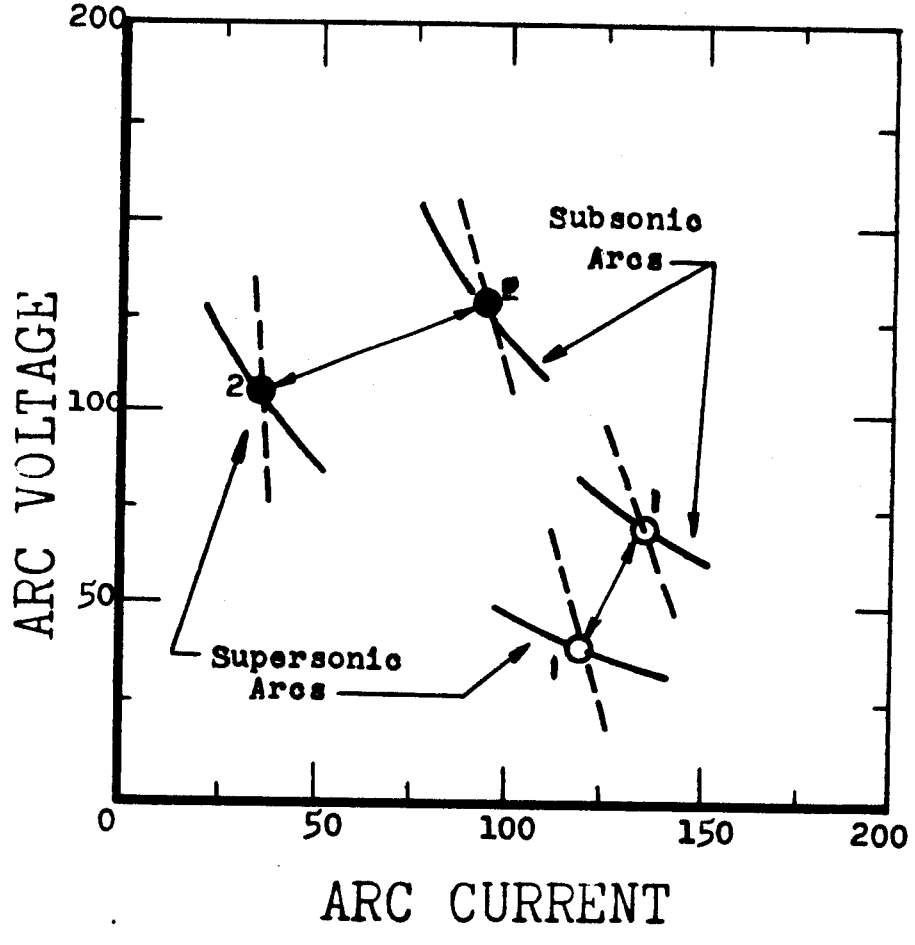

(b) Feasibility Demonstration of Varying Current and Voltage of Subsonic and Supersonic Arcs

Fig. 22

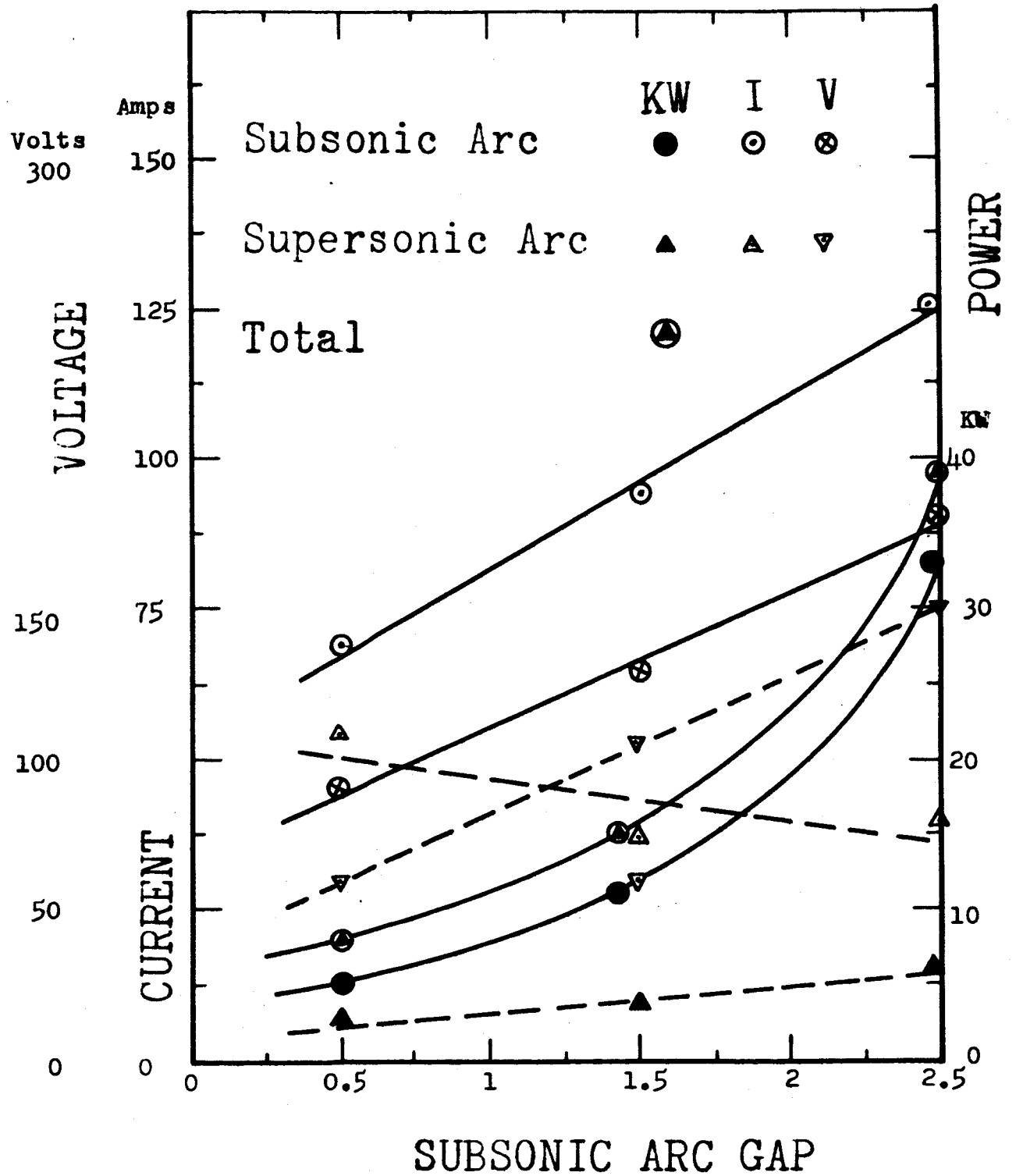

Fig. 23 Power, Voltage, Current Variations in a Double Arc as a Function of Subsonic Electrode Gap

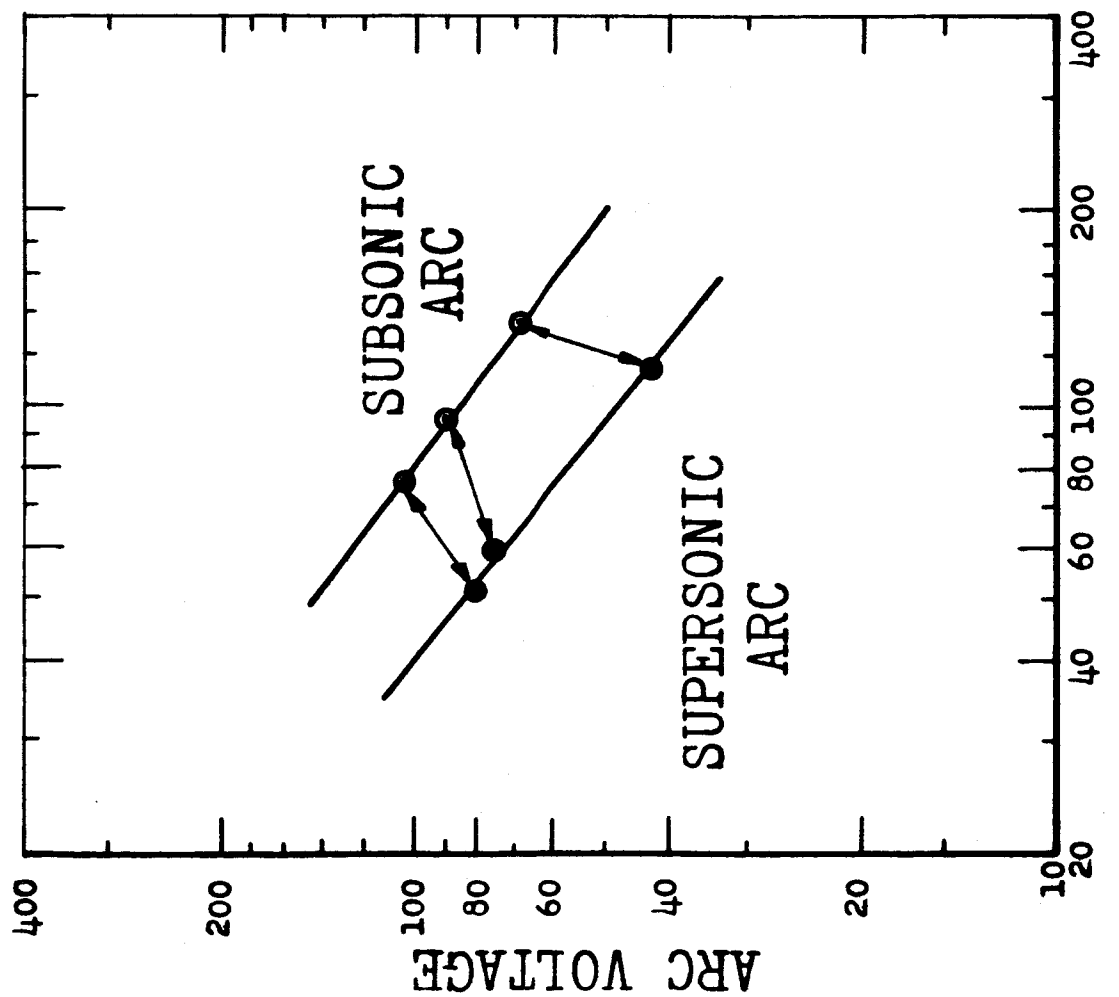

Fig. 24 V-I Characteristics for Double Arc Operation at constant pressure (47 psia)

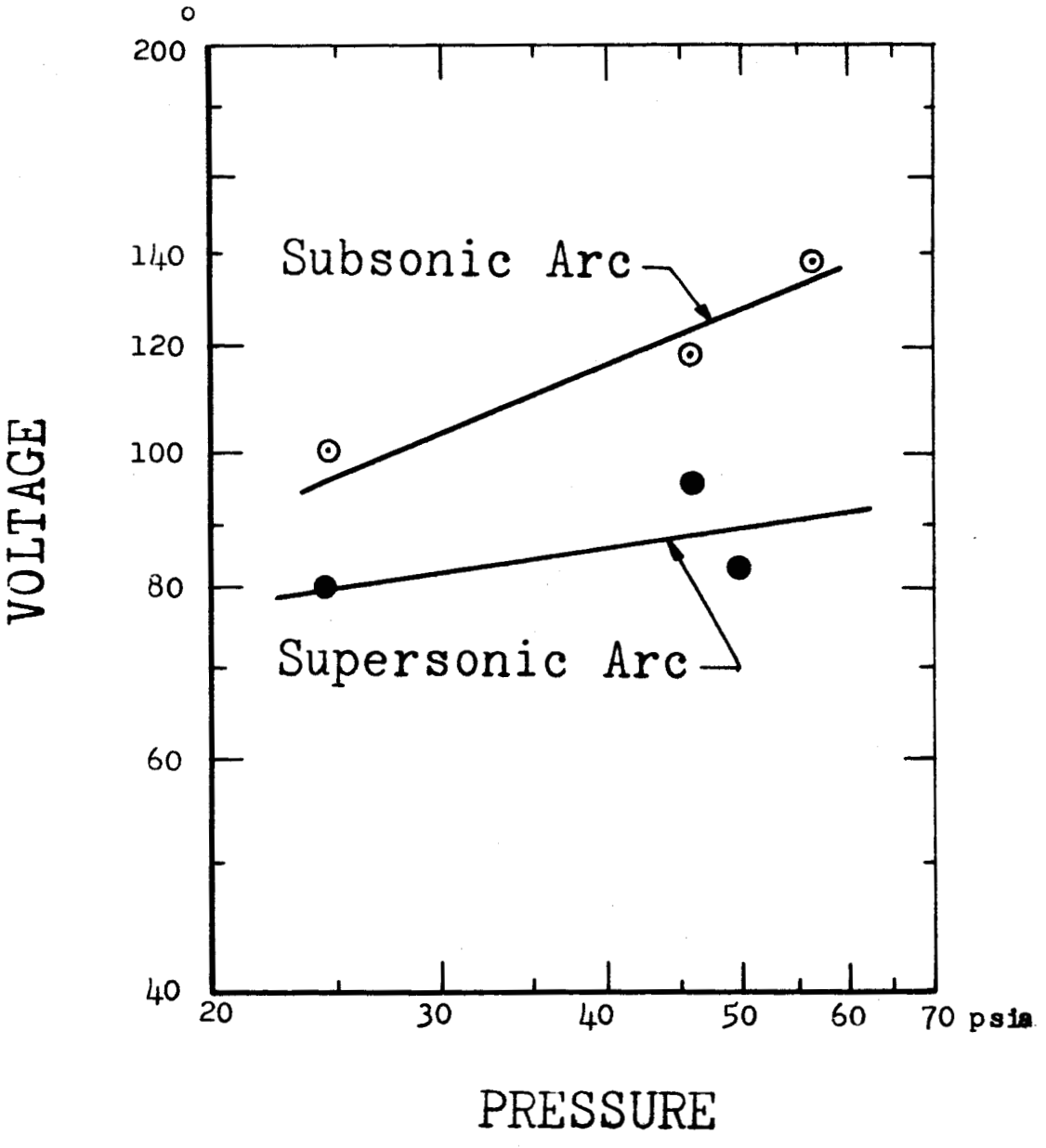

Fig. 25 Double Arc Characteristics - Effect of Pressure at constant current (80 amps for subsonic and 52 amps for supersonic)

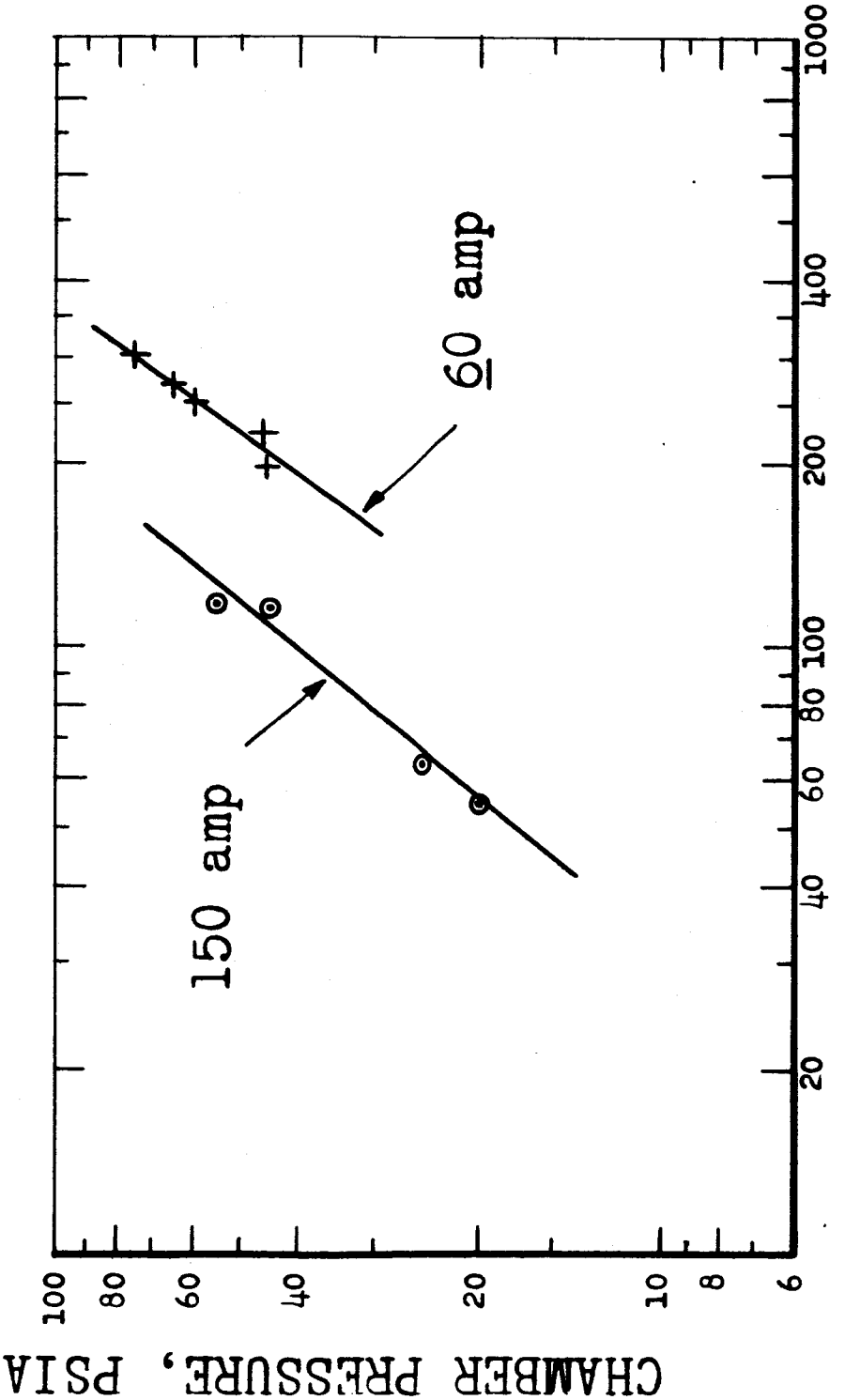

Fig. 26 V-P Characteristics of Subsonic arc alone at constant current level.

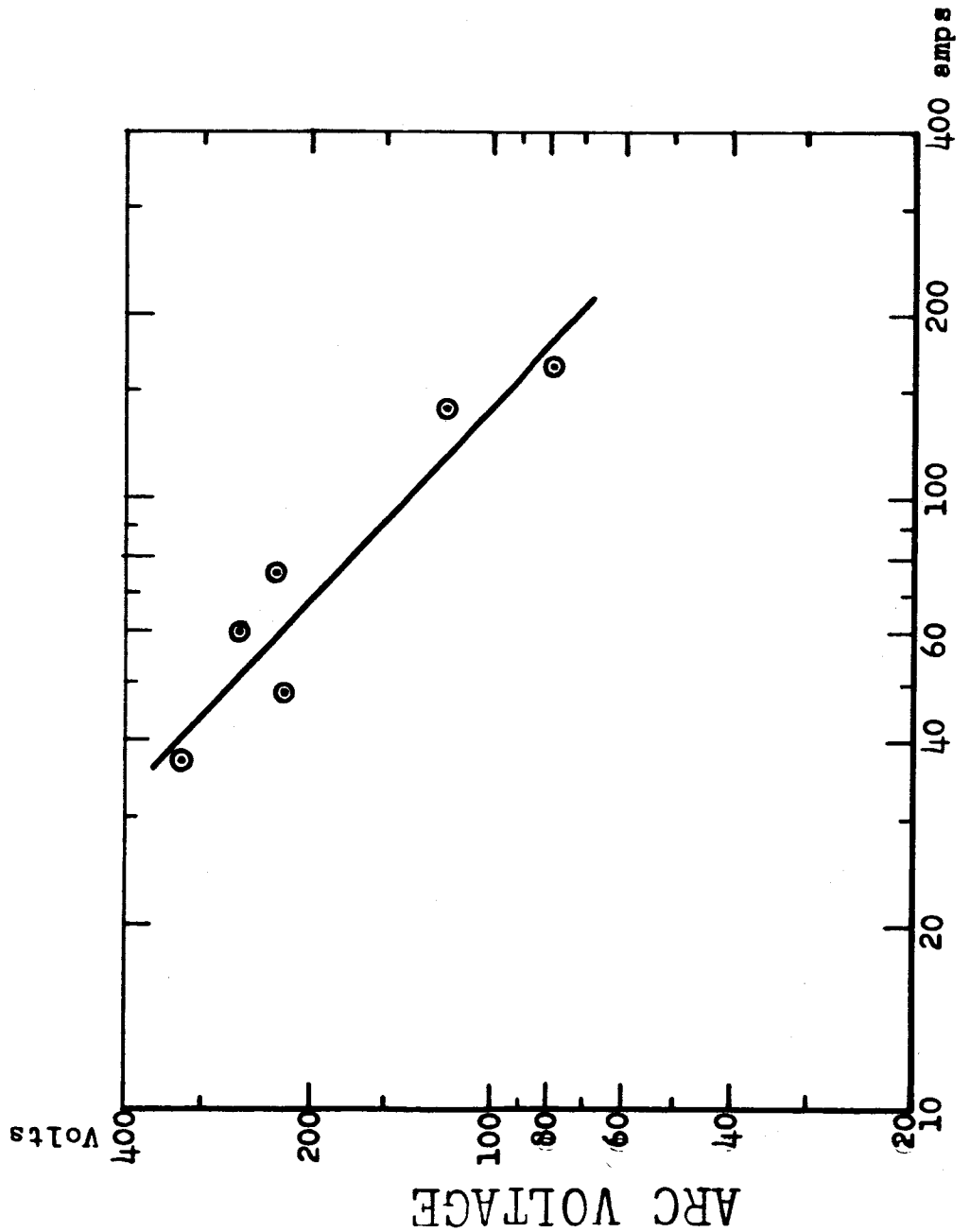

Fig. 27 V-1 Characteristics of the Subsonic Arc Alone at Constant Pressure (50 psia)

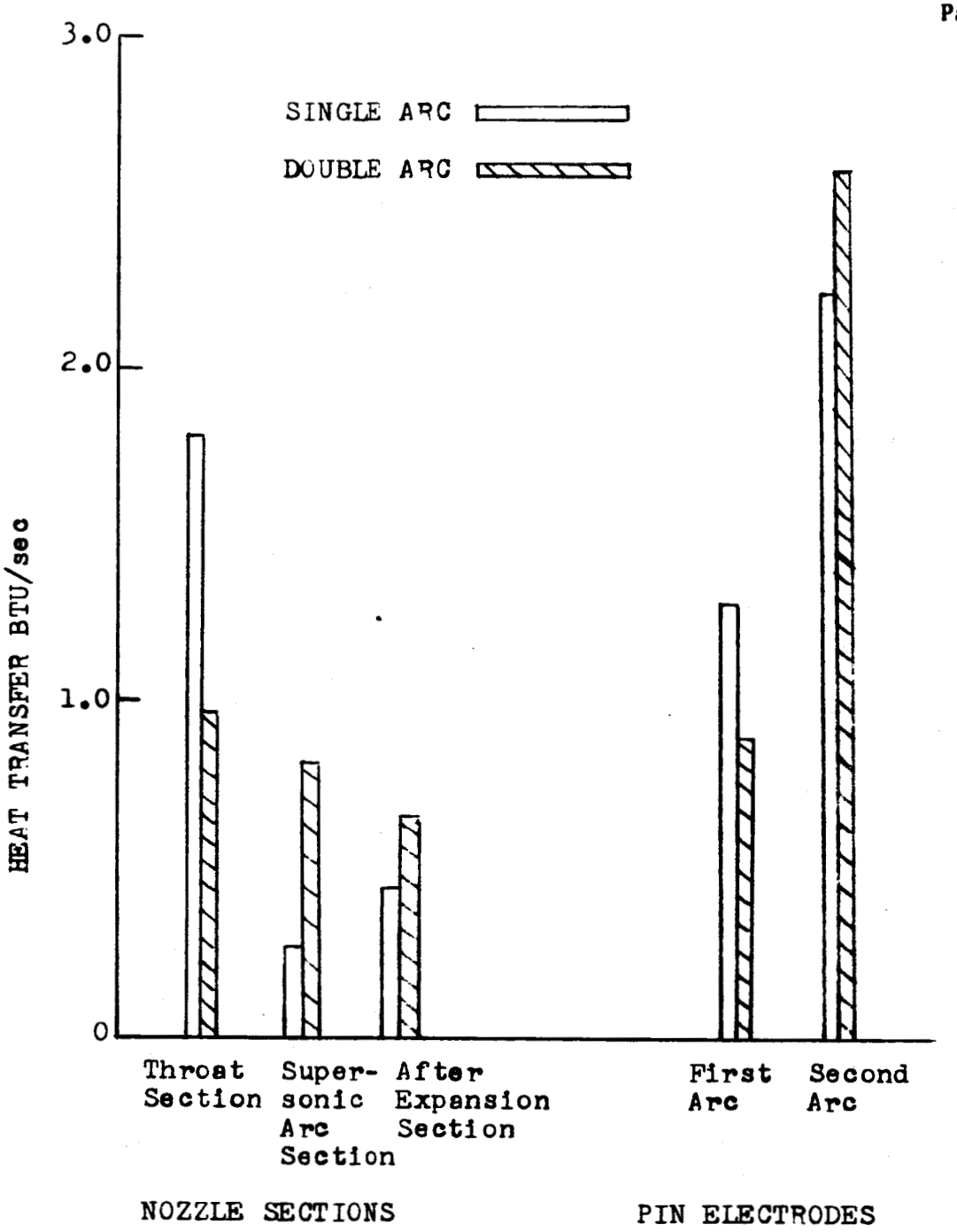

Fig. 28 Heat Transfer to Different Components, for a Double Arc and a Single Arc, at Total Power Input of 12.14 KW (34% in Supersonic) and Chamber Pressure of 24.7 psia.

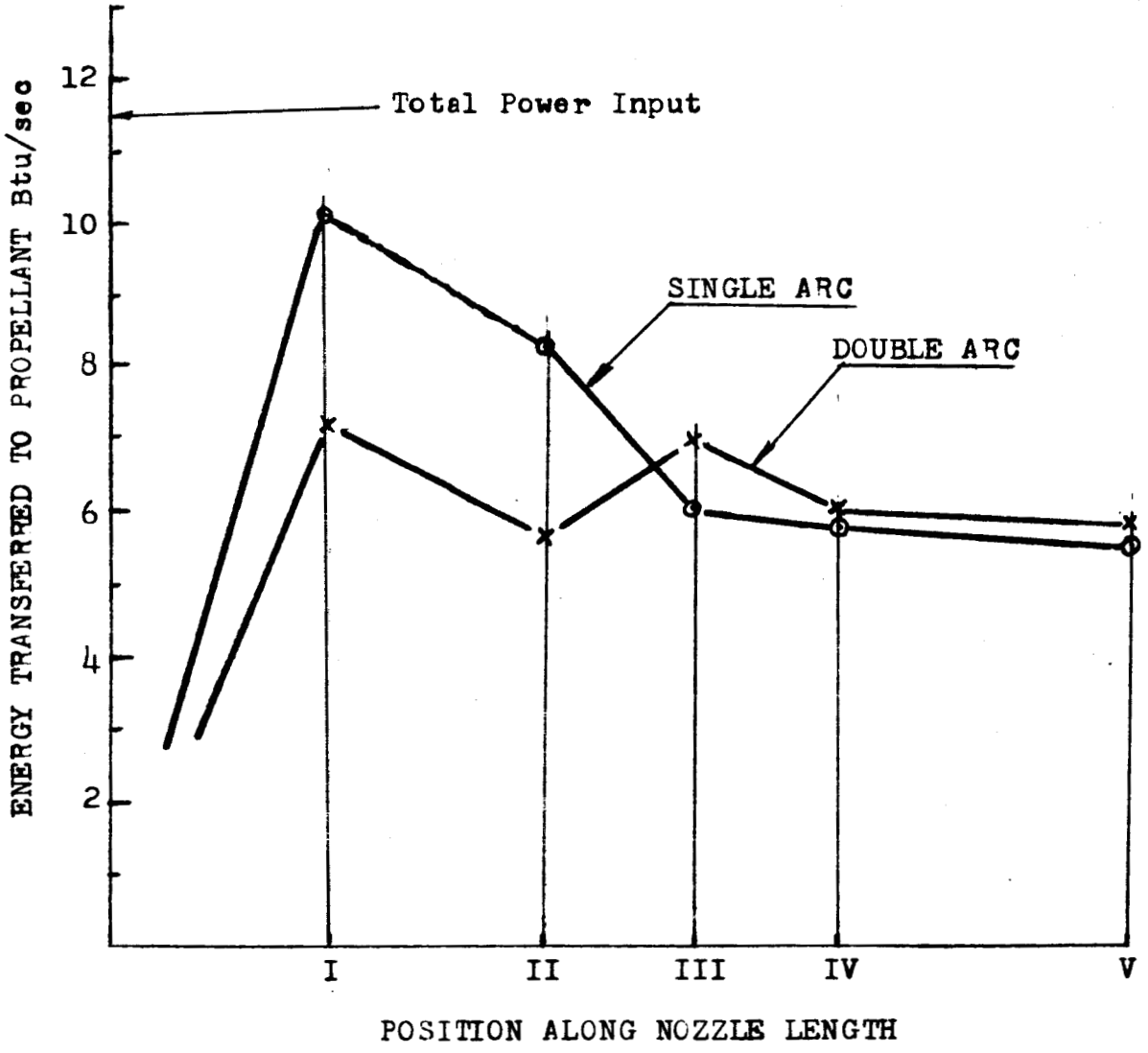

I First Arc Input Less First Arc Electrode Loss
II Less Nozzle Throat Section Loss
III Plus Second Arc Input Less Second Arc Electrode Loss
IV Less Supersonic Arc Nozzle Section Loss
V Less After-Expansion Nozzle Section Loss

Fig. 29 Energy Transfer to Propellant at Different Locations in the Nozzle, for a Double Arc and a Single Arc, Total Power Input of 12.14 KW and Chamber Pressure of 24.7 psia, 34% power in Supersonic Arc.

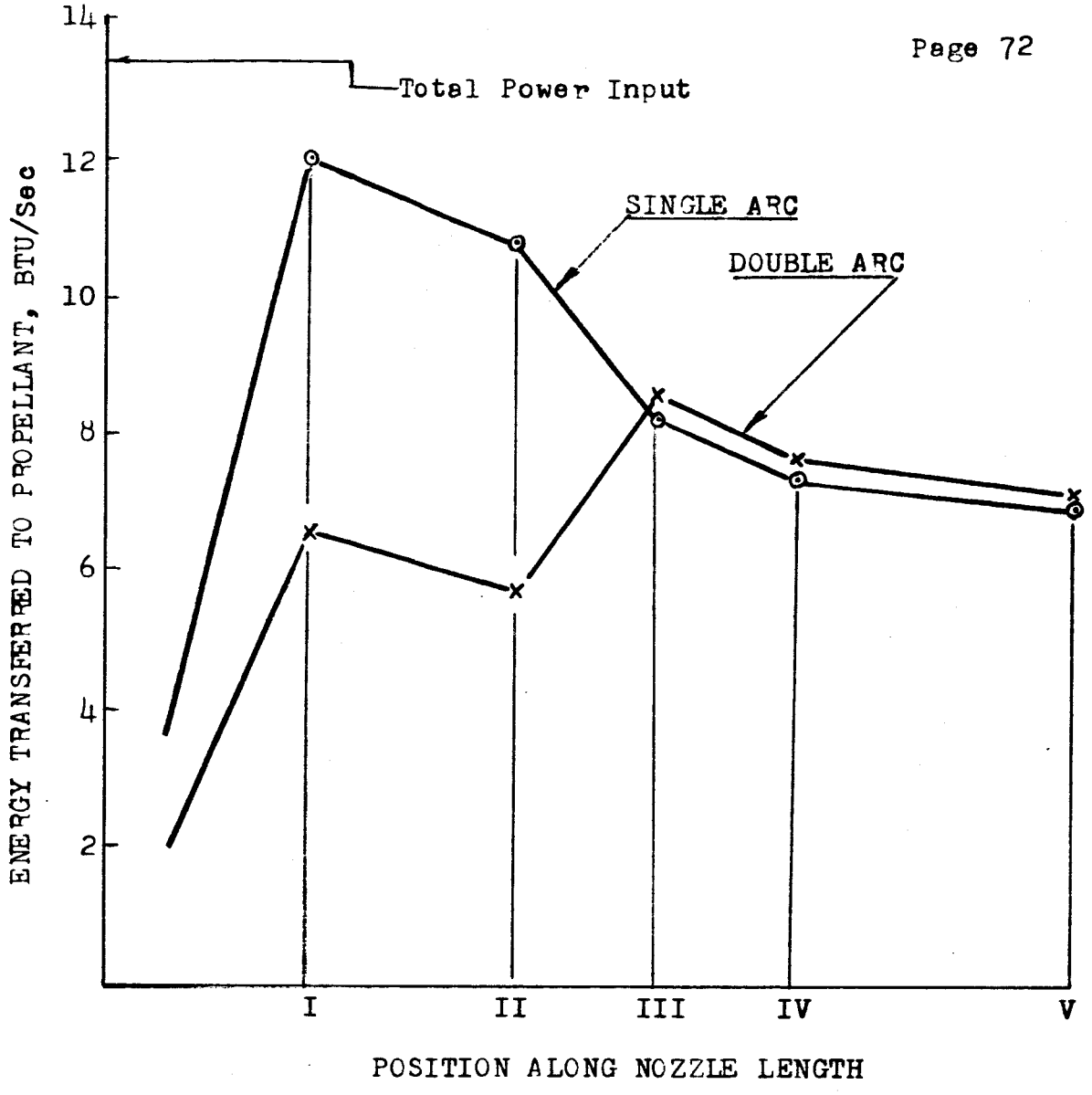

I First Arc Input Less First Arc Electrode Loss
II Less Nozzle Throat Section Loss
III Plus Second Arc Input Less Second Arc Electrode Loss
IV Less Supersonic Arc Nozzle Section Loss
V Less After-Expansion Nozzle Section Loss

Fig. 30 Energy Transfer to Propellant at Different Locations in the Nozzle, for a Double Arc and a Single Arc, Total Power Input of 14.04 KW and Chamber Pressure of 42 psia 41% Power in Supersonic Arc

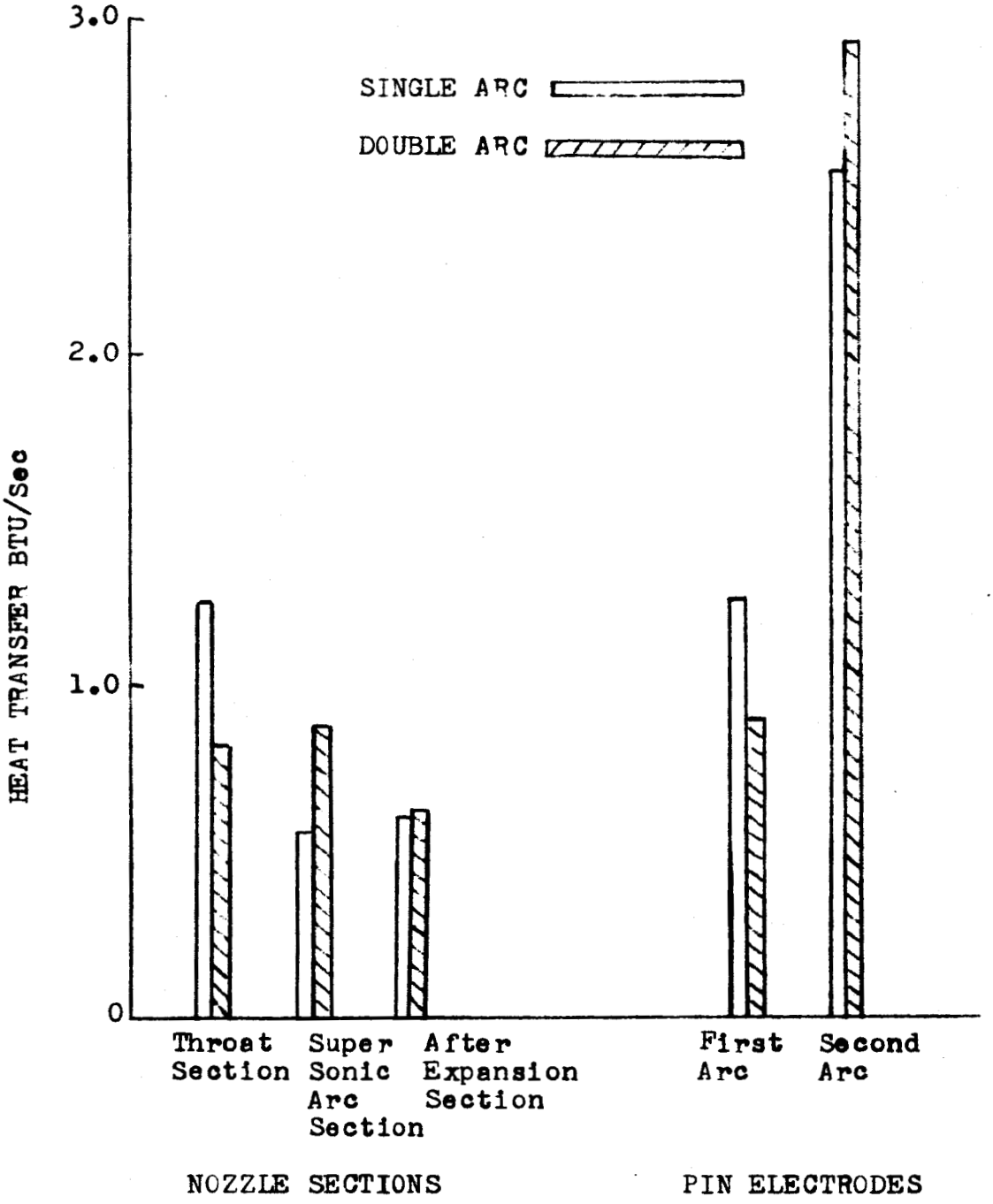

Fig. 31 Heat Transfer to Different Components, for a Double Arc at Total Power of 14.04 KW (41%) in Supersonic) and Chamber Pressure of 42 psia,

APPENDIX I

THERMAL LOSS CHARACTERISTICS

Rubber Hoses

Thermal losses from the rubber hoses connecting various coolant passages was computed. The heat transfer coefficient to the outside, h_o, was calculated from the equations.

$$h_o = 0.24 \left(\frac{\theta}{d}\right)^{0.4}$$

$$q_o = h_o A \theta$$

where θ is the temperature difference between the environment and the outside surface, A, the exposed surface, and d, the outside diameter of the hose.

Assuming water side coefficient of 100 Btu per hr $ft^2{}^oF$ and resistivity of the rubber hose wall, the combined coefficient was calculated as 16.2 Btu per hr $ft^2{}^oF$. The surface temperature difference, θ, may then be expressed by the following equation, in terms of (Δt), which is the total temperature difference between the cooling water and the environmental air,

$$\frac{(\Delta t - \theta)}{\theta} = \frac{16.2}{h_o}$$

Combining this with the expression for h_o, substituting d equal to half an inch, and A equal to .78 sq. ft., it gives

$$\frac{(\Delta t - \theta)}{\theta} = \frac{26.7}{(\theta)\,0.25}$$

$$q_o = 0.476\ (\theta)^{1.25}$$

q_0 was computed for (Δt) varying from 10 to 100°F, and plotted in Fig. 20.

Exposed Engine Surfaces

The total exposed area consisting of exposed engine surface, exposed copper tubes connecting the various engine passages to rubber hoses, and the exposed parts of the thermometer walls, was 0.128 sq. ft. The thermal loss was then calculated from the equation.

$$q_0 = (0.24)\ (0.128)\ (2.53)\ (\theta)^{1.25}$$

Thermal losses are shown in Fig. 20. To illustrate the magnitude of error involved, two examples were taken.

In the first example, with (Δt) of 20°F and heat collection rate of one KW for each of the flow circuits, the above thermal loss was 0.5 percent. For five circuits, this would be 0.25 percent.

In the second example, with (Δt) of 50°F, heat collection rate of one KW for each of the flow currents, the thermal loss was 0.3 percent.

Thermal loss corrections were made when (Δt) was 50°F or more.